For Reference

NOT TO BE TAKEN FROM THIS ROOM

For Reference

NOT TO BE TAKEN FROM THIS ROOM

Ex libris
Universitatis
Albertaensis

The University of Alberta
Printing Department
Edmonton, Alberta

UNIVERSITY OF ALBERTA
LIBRARY

Regulations Regarding Theses and Dissertations

Typescript copies of theses and dissertations for Master's and Doctor's degrees deposited in the University of Alberta Library, as the official Copy of the Faculty of Graduate Studies, may be consulted in the Reference Reading Room only.

A second copy is on deposit in the Department under whose supervision the work was done. Some Departments are willing to loan their copy to libraries, through the inter-library loan service of the University of Alberta Library.

These theses and dissertations are to be used only with due regard to the rights of the author. Written permission of the author and of the Department must be obtained through the University of Alberta Library when extended passages are copied. When permission has been granted, acknowledgement must appear in the published work.

This thesis or dissertation has been used in accordance with the above regulations by the persons listed below. The borrowing library is obligated to secure the signature of each user.

Please sign below:

Date	Signature	Institution

Digitized by the Internet Archive
in 2019 with funding from
University of Alberta Libraries

https://archive.org/details/lsil1969

THE UNIVERSITY OF ALBERTA

[illegible]

by

© [illegible]

A THESIS

SUBMITTED TO THE FACULTY OF GRADUATE STUDIES AND RESEARCH
IN PARTIAL FULFILMENT OF THE REQUIREMENTS FOR THE DEGREE
OF [illegible]

DEPARTMENT OF [illegible]

EDMONTON, ALBERTA

[illegible]

Thesis
1969(F)
119

THE UNIVERSITY OF ALBERTA

THE GAS PHASE EQUILIBRIA AND RELATED THERMODYNAMIC QUANTITIES OF THE THERMAL ION-MOLECULE REACTIONS IN ETHANOL.

by

© MAHMUT TUNCER ISIL

A THESIS
SUBMITTED TO THE FACULTY OF GRADUATE STUDIES
IN PARTIAL FULFILMENT OF THE REQUIREMENTS FOR THE DEGREE
of
MASTER OF SCIENCE

DEPARTMENT OF CHEMISTRY

EDMONTON, ALBERTA
Fall, 1969

UNIVERSITY OF ALBERTA
FACULTY OF GRADUATE STUDIES

The undersigned certify that they have read, and recommend to the Faculty of Graduate Studies for acceptance, a thesis entitled "THE GAS PHASE EQUILIBRIA AND RELATED THERMODYNAMIC QUANTITIES OF THE THERMAL ION-MOLECULE REACTIONS IN ETHANOL" submitted by M. Tuncer Isil in partial fulfilment of the requirements for the degree of Master of Science.

ABSTRACT

The gas phase solvation reactions of the proton with ethanol molecules at high pressures and in the temperature region of (25-400°C) were investigated. These were condensation type thermal ion-molecule reactions which were allowed to occur in the high pressure electron impact ion source of a quadrupole mass spectrometer. The pulsing technique and the normal continuous operational mode of the quadrupole mass spectrometer were both employed.

The occurrence of the general reaction,

$$H^+(C_2H_5OH)_{n-1} + C_2H_5OH \rightleftarrows H^+(C_2H_5OH)_n$$

has been confirmed from a study of ions present in the system.

The equilibrium constants of some of the reactions in the sequence were attempted to determine and the related thermodynamic quantities derived at various temperatures. A significant variance of the equilibrium constants with pressure was observed. The equilibrium constants were also found as a decreasing function of temperature and the size of cluster (n).

Since the reactions were very fast, the pseudo first order rate constants of the reactions could not be evaluated from the normalized ion intensity versus reaction time curves. Because of the limited time we had, this evaluation by, for example, dilution with a noble gas, has been left to future projects.

ACKNOWLEDGEMENTS

I would like to express my appreciation to Dr. Paul Kebarle for his advice throughout the course of this work.

I wish to acknowledge the co-operation of Dr. Masakazu Yoshida in part of the work.

My sincere appreciation goes to Mrs. Mary Waters for typing the manuscript.

The financial assistance provided by the University of Alberta is gratefully acknowledged.

I should like to thank Drs. David A. Durden and Anthony Good for their valuable advice and the reading of the draft copy.

TABLE OF CONTENTS

LIST OF TABLES

LIST OF FIGURES

1. INTRODUCTION

1:1 The Scope of Present Study

The present study was designed to investigate the gas phase equilibria and kinetics of the "thermal ion-molecule" reactions in ethanol in the high pressure range of 0.1 - 5.0 torrs and at temperatures in the 20 - 400°C range.

The reactions were studied in a high energy (3000 eV) electron beam impact, high pressure quadrupole mass spectromter. The reaction times were set and measured by means of a pulsing technique. Charged molecular clusters such as mono and poly solvated protons $[(C_2H_5OH)_nH^+]$ were observed. Some preliminary values of the equilibrium constants of the solvation reactions were evaluated.

In the following sections a brief introduction to condensation type ion-molecule reactions and a literature survey are given.

1:2 Ion-Molecule Reactions

The first detection of ion-molecule reactions coincided with the beginning of mass spectroscopy. In 1913 J. J. Thompson [1] observed a line corresponding to a particle of mass to charge ratio m/e = 3 in the product stream of a hydrogen discharge. In 1916 Dempster[2] showed

that this m/e = 3 particle was the triatomic hydrogen species H_3^+ and that it was truly the product of a secondary reaction. Through the years prior to 1950 there was little interest in ion molecule reactions. However, a few studies were done. For example, Mann, Hustralid, and Tate [3] in 1940 showed that the oxonium ion can be formed in the reaction,

$$H_2O^+ + H_2O \rightarrow H_3O^+ + OH$$

In 1940 Eltenton [4] discovered the reaction,

$$CH_4^+ + CH_4 \rightarrow CH_5^+ + CH_3$$

which was later re-examined by several other researchers.

The recent rapid developments in the field of ion-molecule reactions were initiated by V. L. Tal'roze, and A. K. Lyubimova [5] in the Soviet Union, and Stevenson, Schissler,[6] Field, Franklin, and Lampe [7] in the United States.

Several types of ion-molecule reactions have been observed to occur and these have been discussed in a number of texts.[8,9,10]

In this work we will consider only condensation reactions since the study concerns itself only with reactions of this type.

1:3 Condensation Ion-molecule Reactions.

Condensation ion-molecule reactions essentially include all reactions in which a strongly bound complex, which may or may not be stablized by collision, is produced.

$$AB^{+} + CD \rightarrow (ABCD^{+})^{*}$$

$$(ABCD^{+})^{*} \rightarrow \text{Fragmentation Products}$$

or

$$(ABCD^{+})^{*} \xrightarrow{M} ABCD^{+}$$

The ion product generally has higher molecular weight than the primary or precursor ion (AB^{+}). The intermediate reaction complex $(ABCD^{+})^{*}$ can be collisionally stabilized at sufficiently high pressures.

A very large number of ion-molecule reactions with different types of chemical bonding fall into this category. Therefore, it is convenient to make the subclassification shown below.

(A) Rearrangement Reactions

These reactions are condensation ion-molecule reactions in which a significant rearrangement takes place among the covalent bonds of the reactants, resulting in new chemical bonds. This type is often observed with unsaturated hydrocarbons i.e.,

$$C_2H_4^{+} + C_2H_4 \rightleftarrows (C_4H_8^{+})^{*} \xrightarrow{C_2H_4} C_4H_8^{+}$$

In the reaction given above the intermediate complex $(C_4H_8^+)^*$ has a large excitation energy due to bond formation. This energy is distributed in its vibrational and rotational modes and can bring about dissociation to the initial reactants, or a decomposition to $(C_3H_5^+ + CH_3)$ and $C_4H_7^+ + H)$. Collisions of the excited complex with the gas molecules remove some of the excess energy and can result in stabilization leading to the formation of $(C_4H_8^+)$. At high pressures the reactions can even proceed further and consequently higher order condensations may be observed. For example,

$$C_4H_8^+ + C_2H_4 \rightarrow (C_6H_{12}^+)^* \xrightarrow{C_2H_4} C_6H_{12}^+$$

(B) Clustering Reactions.

Reactions in which the bonding is mainly due to ion-dipole and induced dipole interactions are called clustering reactions. The reactions of inorganic ions with polar molecules to form complexes are typical examples of such processes:

$$K^+ + H_2O \overset{M}{\rightleftarrows} K^+(H_2O)$$

$$K^+(H_2O) + H_2O \overset{M}{\rightleftarrows} K^+(H_2O)_2$$

$$Cs^+ + H_2O \rightleftarrows Cs^+(H_2O)$$

$$I^- + H_2O \rightleftarrows I^-(H_2O)$$

(C) Intermediate Reactions between the First Two Classes (A,B)

In this type of reaction the bonding of the complex is partially covalent and partially ionic in character. Examples of this type can be given as follows:

$N_2^+ + N_2 \rightarrow N_4^+$

$O_2^+ + O_2 \rightarrow O_4^+$

$O_6^+ + O_2 \rightarrow O_8^+$ (mostly polarization forces)

$F^- + HF \rightarrow (FHF^-)$ (covalent + ionic bonding)

1:4 The Methods and Techniques of Investigations.

The mass spectrometer has been the most powerful and unique tool for the observation and detection of ion-molecule reactions. The conceptual simplicity of this approach lies on the ability to identify the reactant and the product ions directly. Unfortunately it is impossible to determine the neutral products by mass spectrometry, therefore their nature must be inferred.

In mass spectroscopic studies of ion-molecule reactions by conventional internal ionization techniques (Figure 1:1), the ion-molecule reactions are allowed to occur in the primary ion source. Therefore the reactant ions are subject to acceleration by the electric field required to withdraw the ions out of the ion source. Consequently the cross-sections of ion-molecule reactions are determined for variable velocities of these primary

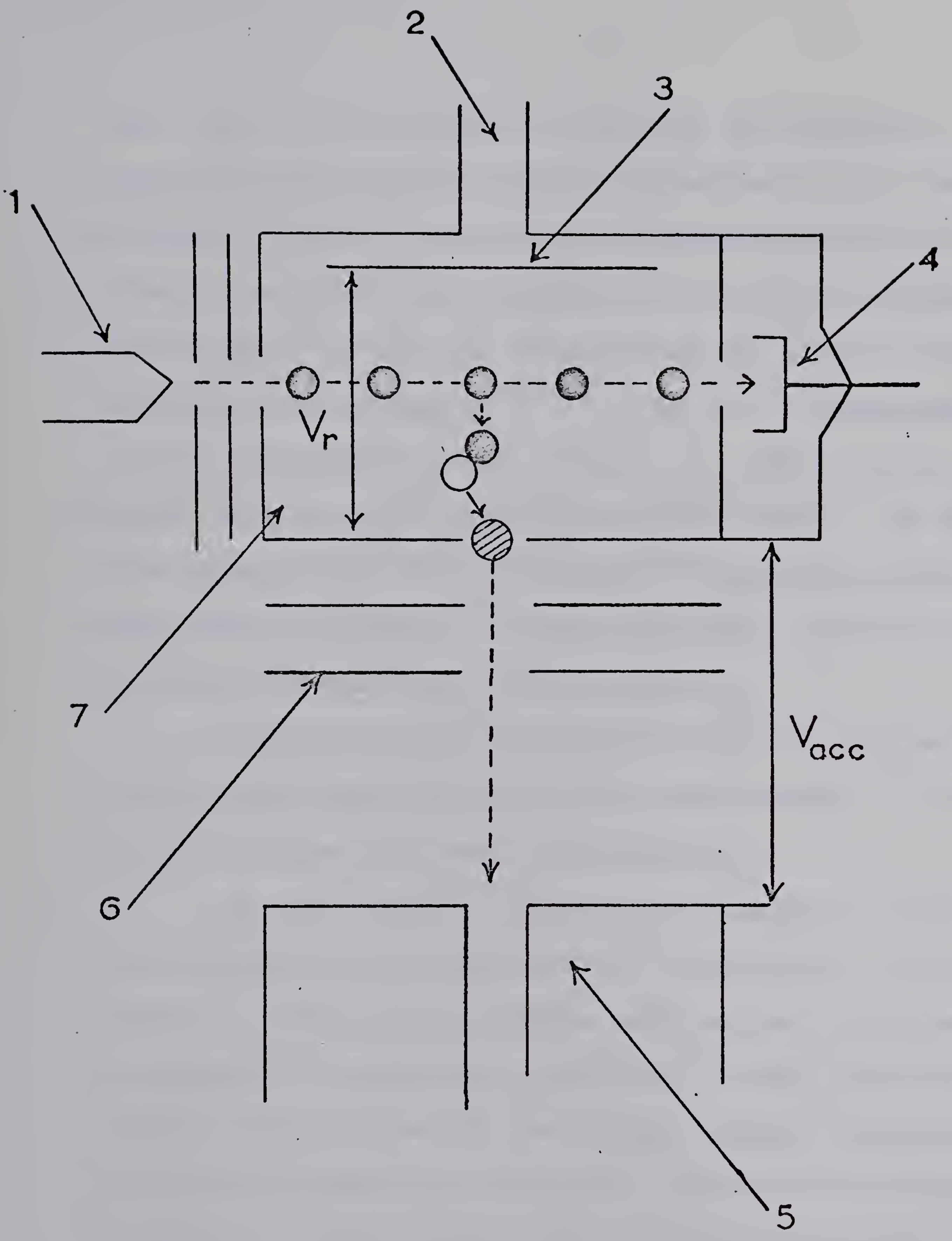

◍ Prime ion ▨ Sec ion, ○ Gas molecules

FIGURE 1:1 APPARATUS: (1) filament; (2) gas inlet; (3) repeller; (4) electron trap; (5) mass analyzer; (6) ion withdrawal electrodes; (7) the ion source.

ions. The cross sections so obtained are dependent on the field strength and the distance travelled by the ions. Extensive investigations of the dependence of the ion-molecule reaction cross sections on the field strength have been carried out but the results have not been in agreement. Stevenson and colleagues [12,13] found an $E^{-\frac{1}{2}}$ dependence for a number of simple systems which is compatible with the predictions from the ion-induced dipole model. On the other hand, Field [14,15] found an E^{-1} dependence while Hamill and co-workers [16] found the energy dependence was a function of the final ion exit energy.

Electronic space charge and mass discrimination effects have been reported by Ryan and Futrell [17] as possible causes for these discrepancies.

In the external ionization techniques (Figure 1:2) the primary ions are prepared in a preliminary ion-source outside of the reaction chamber and can be introduced into the chamber at controlled velocities. More direct and accurate observations of the kinetic energy dependence of the ion-molecule reactions are therefore possible. A number of studies using this technique both with [18,19,20] and without [21,22,23] preliminary mass selection of the reactant ion have been reported. Although several attempts have been made, it has not been possible to obtain primary ion beams of well-defined energy below the critical region of 0.5 - 1.0 eV. Because of this limitation which

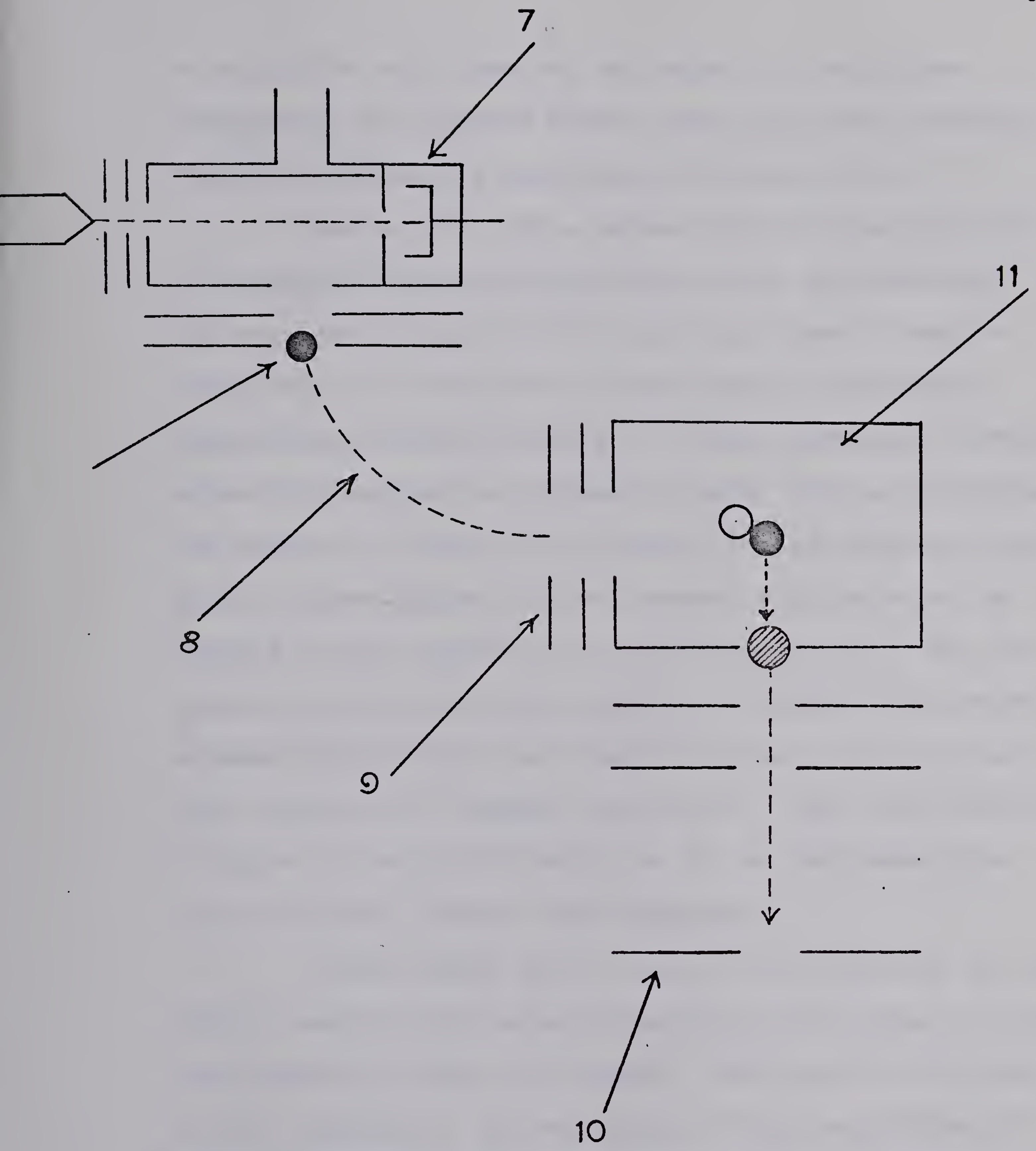

FIGURE 1:2: (7) primary ion source; (8) preliminary mass analyzer; (9) retarding electrodes; (10) second mass analyzer; (11) reaction chamber.

is valid for both internal and external ionization techniques, no accurate kinetic data has been available for the ion-molecule reactions of thermal ions.

However, in 1960 a pulsed mode of operation of an internal ionization source was first described by Tal'roze and Frankevich.[24] This could permit the investigation of ion-molecule reactions at velocities approaching thermal velocity. In this technique a short pulse of electrons is allowed to enter into a field-free ion source to produce the primary ions by electron impact. After a known period of time another voltage pulse is applied to the repeller to push the ions out of the ion source and into the mass analyzer. In the time interval between the electron and repeller pulses the ions react under essentially thermal conditions. The rate constants of these ion-molecule reactions can be evaluated from the ion current versus time dependence.

In the recent past, the pulsing technique has been widely used in both magnetic deflection and time of flight instruments to study the thermal ion-molecule reactions at low pressures. An extension of this technique to apply to high pressures has been developed in this laboratory.

1:5 The Choice of Pressure Range

Due to the laws governing chemical kinetics it is well known that the reaction rates are dependent on the

concentrations and consequently on the partial pressures of the reactants. Therefore at low pressures the only reactions which can be detected are the ones with very high rate constants. Also, reactions which require third body stabilization, like the clustering reactions mentioned earlier, cannot be studied at low pressures. It is necessary to go to higher pressures in order to study reactions of this type. It is obvious that, as far as the design of the instruments is concerned, some modifications relative to conventional low pressure instruments should be made. These modifications are essentially made on two closely related parts of the instrument.

(A) Modification of Ion Sources.

To resolve the problem of having an ion source which has a high inside gas pressure from disturbing the low pressure of the vacuum chamber, large low pressure electron beam entrance and ion exit slits must be replaced by smaller ones. This replacement reduces the over-all conductance of the ion source. Generally one also increases the pumping capacity of the vacuum system which pumps the ion source.

(B) Modifications of Ionizing Radiation Sources

Because of high ion-source pressures the electrons

of energies in the 10.0 - 100.0 eV range are severely scattered and attenuated by the gas molecules. The problem of attenuation can be overcome by the use of more penetrating radiation such as α and γ rays or a highly accelerated beam of protons.

In the present instrument an electron gun producing a high energy (3000 eV) electron beam has been utilized. As an additional characteristic, electrostatic focussing has been applied in the design of the electron gun optics. The electron gun also allows pulsing of the electron beam, which is not possible with an α source. The mass spectrometer developed along these lines is fully described in the second part (Part 2, Apparatus).

1:6 Evaluation of Equilibrium Constants, Other Thermodynamic Quantities, and Rate Constants from Mass Spectrometer Measurements.

(A) Thermodynamic Quantities

Let us consider the condensation sequence,

$$A^+ + B \overset{M}{\rightleftarrows} AB^+ \qquad (1)$$

$$AB^+ + B \rightleftarrows AB_2^+ \qquad (2)$$

$$AB^+_{n-1} + B \rightleftarrows AB^+_n \qquad (3)$$

For the purpose of the discussion we will assume that the reverse steps of the initial reactions are slow.

Under these conditions the forward reaction proceeds only and the cluster grows. At a certain size of the cluster the rate of the reverse reaction must become rapid since the bonding forces holding the cluster together generally decrease as the size of the cluster increases. At the point where the rates of the reverse reactions become comparable with the rates of forward reactions condensation equilibrium is achieved. Under these conditions equation (4) should hold.

$$K_p = \frac{P_{AB_n^+}}{(P_B)(P_{AB_{n-1}^+})} \qquad (4)$$

With the mass spectrometer the partial pressures cannot be measured. However, the partial pressure ratio of the ions can be replaced by the intensity ratio of the corresponding ions. Thus the equation takes the form (5),

$$K_p = \frac{I_{AB_n^+}}{(P_B)(I_{AB_{n-1}^+})} \qquad (5)$$

In order to obtain ion intensities at equilibrium one must wait until the ionic concentration becomes constant. The ionic intensities are observed as a function of time after an initial ionizing electron pulse.

Equilibrium is assumed to be reached if the relative intensities become constant after some time t.

Once the equilibrium constants at a number of different ion source temperatures are known, the ΔH values of reactions in the sequence can be estimated from the slopes of the equilibrium constant (K_p) versus (1/T) curves using the Van't Hoff equation.

One can easily find out the standard free energy changes (ΔG°) of the reactions by utilizing the equation (6),

$$\Delta G^\circ = - RT.\ln K_p \tag{6}$$

The remaining thermodynamic quantity (ΔS) may be evaluated by putting the other previously known thermodynamic quantities into the equation (7)

$$\left(\frac{\delta \Delta G}{\delta T}\right)_P = -\Delta S = \frac{\Delta G - \Delta H}{T} \tag{7}$$

(B) Rate Constants

Let us consider a first order reaction sequence,

$$A_1^+ \xrightarrow{\gamma_1} A_2^+ \xrightarrow{\gamma_2} A_3^+ \longrightarrow \ldots\ldots \longrightarrow A_n^+ \tag{8}$$

where γ_n is the first order reaction rate constant. In this case the ion intensities at time t are given by the equations (9), (10), and (11)

$$I_1 = I_1^\circ.e^{-\gamma_1 t} \tag{9}$$

$$I_2 = I_1^{\circ}\cdot\gamma_1 \left[\frac{e^{-\gamma_1 t}}{\gamma_2 - \gamma_1} + \frac{e^{-\gamma_2 t}}{\gamma_1 - \gamma_2} \right] \tag{10}$$

$$I_n = I_1^{\circ}\cdot\gamma_1\cdot\gamma_2\cdot\cdots\cdot\gamma_{n-1} \left[\left(\frac{e^{-\gamma_1 t}}{(\gamma_2-\gamma_1)\ldots(\gamma_n-\gamma_1)} \right) + \ldots\ldots + \left(\frac{e^{-\gamma_n t}}{(\gamma_1-\gamma_n)\ldots(\gamma_{n-1}-\gamma_n)} \right) \right] \tag{11}$$

Evaluation of the rate constants from these time dependent functions of ion intensities would be an algebraic operation. For the sake of simplicity brief descriptions of only three algebraic methods of estimating the rate constants of condensation reactions will be given below.[25]

(1) The logarithmic plot method consists of two succeeding procedures. Firstly one obtains the plots of the logarithm of ion current versus time, which because of their first order kinetic character, are straight lines. Secondly one calculates the rate constants from the slopes of these straight lines. This method can be applied to any ion (A_n^+) where the intensities of all precursor ions (A_{n-1}^+, A_{n-2}^+,....,A_1^+) are vanishingly small. In cases where this condition is not satisfied the rate constants cannot be determined accurately even if the log plot appears to give a constant slope since the ion (A_n^+) is still produced from A_{n-1}^+, etc. Consequently

the methods "t_{max}" and "Graphical Integration" must be employed for such cases.

(2) The second method is "t_{max}". If we let "t_{max}" be the time at which the intensity of a given ion (I_n) reaches a maximum, the first differential of (I_n) with respect to t_{max} should be zero. By performing these algebraic operations (differentiation and setting the differential equal to zero) one obtains a new equation which is a function of "t_{max}" and the (γ) values. If the γ_1 to γ_{n-1} values are known, γ_n can be easily evaluated.

(3) The third "Graphical Integration" method depends on the relationship,

$$I_{n+1} + I_{n+2} + I_{n+3} + \ldots\ldots = \gamma_n \int_0^t I_n . dt \qquad (12)$$

The left hand side is a sum of ion currents of all product ions in the reaction sequence with index higher than (n), which are present at the time (t).

In this method, as can be seen in the above relationship, it is necessary to perform the graphical determination of the definite integral ($\int_0^t I_n . dt$) from ion intensity-time curves. The sum of products ($I_{n+1} + I_{n+2} + \ldots\ldots$) are then plotted versus the integral, and a straight line with a slope of γ_n is obtained.

The rate constants in all three methods thus may be

evaluated by utilizing the relationship,

$$K_n = \frac{\gamma_n}{\text{Concentration of neutral reactant}}$$

1:7 Literature Survey

The ion-molecule reactions of the lower alcohols have been the subject of several investigations. Although much is known about the methanol system, little detailed information is available about ethanol.

Tal'roze [26] obtained ionization efficiency curves of $C_2H_5OH^+$ (m/e = 46) and $C_2H_5OH_2^+$ (m/e = 47) by employing internal ionization techniques at an ethanol pressure of 4×10^{-4} torr. In this study the modulation of electron retarding potential, and resonance amplification of the ion current at the frequency of this modulation were also employed. He compared these curves and concluded that, $C_2H_5OH^+$ (m/e = 46) was a precursor of $CH_3CH_2OH_2^+$ (m/e = 47).

Ryan, Sieck, and Futrell [27] published ionization efficiency curves for the ions CH_3CHOH^+ (m/e = 45), $CH_3CH_2OH^+$ (m/e = 46), $CH_3CH_2OH_2^+$ (m/e = 47) and reached the conclusion that, CH_3CHOH^+ is the only important precursor of $CH_2CH_2OH_2^+$. In this investigation the internal ionization technique was employed for low ion source concentrations such as 2.4×10^{13} mol cc^{-1}.

Two years later Futrell, Sieck, and Abramson [28]

studied this system in a single stage, high pressure mass spectrometer at various field strengths and ionizing voltages. The results were also correlated with the data obtained from a tandem apparatus using external technique and having a primary beam mass-energy selection capability. In the tandem instrument the ions had nominally 0.3 eV of translational energy and therefore were not truly thermal. The authors modified their previously mentioned conclusions on these newer data. They concluded that all three major primary ions ($C_2H_5OH^+$, $C_2H_4OH^+$, and CH_2OH^+) transfer protons to ethanol leading to the formation of ($CH_3CH_2OH_2{}^+$). They also observed at elevated pressures the formation of higher-order clusters corresponding to solvated proton structures.

Russell and Chupka [29] examined the high pressure mass spectrum of ethanol by use of photoionization. The advantages of the photoionization technique over electron impact have been explained in detail by Koyano, Omura, and Tanaka.[30] These are firstly the lack of unimolecular fragmentation of the parent ion at selected photon energies, and secondly the absence of a hot filament, which enables one to get higher pressures without suffering pyrolysis. The clustering reactions were examined as a function of ion-source pressure. Equations for the determination of reaction cross-sections were developed,

and ionization efficiency curves were also obtained for the parent ion, and the mono, di, tri-solvated protons. They concluded that the bond formed when a $C_2H_5OH_2^+$ (m/e = 47) ion condenses with an ethanol molecule is stronger than the bond formed by the subsequent condensation reactions. The conclusion has been also drawn that intermolecular energy transfer and internal energy of the reactant ions would have appreciable effects on the condensation reactions in ethanol.

Bansal and Freeman [31] investigated the "radiation-sensitized pyrolysis" of ethanol vapour. Samples were irradiated with a ^{60}Co (γ-ray) source at a dose of 1.3×10^{20} eV/g at 350°C and in a high pressure range of 10^2 to 10^3 torr. The measurements were based on neutral product analysis. They observed that diethyl ether and water were formed, and that the yield of ether was unaffected by the presence of propylene (as a free radical scavenger) and sulphurhexafluoride (as an electron scavenger), but was decreased by the presence of ammonia (as a positive ion scavenger). On this basis they proposed a mechanism of ether formation via charged molecular clusters such as $(C_2H_5OH)_nH^+$ shown below.

$$C_2H_5OH \rightsquigarrow C_2H_5OH^+ + e^- \qquad (14)$$

$$C_2H_5OH^+ + C_2H_5OH \rightarrow C_2H_5OH_2^+ + CH_3CHOH \qquad (15)$$

$$C_2H_5OH_2^+ + C_2H_5OH \rightleftarrows (C_2H_5OH)_2H^+ \qquad (16)$$

$$(C_2H_5OH)_2H^+ \rightarrow (C_2H_5)_2OH^+ + H_2O \qquad (17)$$

$$(C_2H_5)_2OH^+ + C_2H_5OH \rightarrow (C_2H_5)_2O + C_2H_5(OH)_2^+ \qquad (18)$$

$$(C_2H_5OH)_2H^+ + C_2H_5OH \rightleftarrows (C_2H_5OH)_3H^+ \qquad (19)$$

$$MH^+ + e \rightarrow \text{Neutralization} \qquad (20)$$

Reaction (14) represents the radiolysis and resulting ionization of ethanol vapour. Reaction (15) is basically a proton transfer reaction between ionized and neutral ethanol molecules. Charged molecular clusters are formed in the reversible reactions (16) and (19). Reaction (17) represents the normal pyrolysis of the ionic species and has an equivalent reaction in methanol.

A few similar type studies were done in this laboratory for different central ions and for various kinds of ligand molecules.

P. Kebarle, R. N. Haynes, and J. G. Collins [37] in 1967 studied the ions in irradiated-water-methanol vapour mixtures and showed that the principal species were clusters $(CH_3OH)_m(H_2O)_wH^+$. The authors found that methanol was taken up preferentially in clusters of small size, and the preference for methanol decreases with size of the cluster. Water was taken up preferentially in larger clusters. The data indicated that, in a small cluster ($m+w = 3,4,$ or 5) the methanol molecules were equivalent among themselves, as were the water molecules. Extrapol-

ation of the data for cluster containing only the proton and one solvent molecule predicted 11 kcal/mole for the difference between the proton affinity of methanol and water.

P. Kebarle [38] in 1968 published studies on systems in which the central ions were NH_4^+, H_3O^+, Na^+. The solvating agents were NH_3 and H_2O molecules. The comparative solvation of Cl^-, BCl^-, and B_2Cl^- by water was described. In a study of competitive solvation of $CH_3OH_2^+$ by water and methanol, it was found that methanol was more strongly solvating at close range of the ion. At larger distances water was taken up preferentially. The NH_4^+ ion showed a distinct inner shell of four solvent molecules. NH_3 was taken up into this shell while H_2O was taken up preferentially into the outer shell.

S. K. Searles and P. Kebarle [39] in 1969 evaluated the thermodynamic constants $\Delta H_{n-1,n}$ $\Delta G^\circ_{n-1,n}$ and $\Delta S^\circ_{n-1,n}$ for the reaction

$$K^+(H_2O)_{n-1} + H_2O \rightleftarrows K^+(H_2O)_n$$

proceeding in the gas phase for n=1 and n=6. The equilibria were investigated in a water vapor pressure range of 0.3 - 6.0 torr and at temperatures - 11 to 390°C. The K^+ ions were produced by thermoionic emission in a filament chamber and then were equilibrated with the water vapor in the reaction chamber. The relative ionic

concentrations were measured by a magnetic mass spectrometer. A comparison was made regarding the energy differences between the experimental $\Delta H^{\circ}_{n-1,n}$ values and the theoretical potential energy values which was based on simple electrostatic model calculations.

It was found that the theoretical values were in fair agreement with the experimental results. The statistical mechanical calculation of the $\Delta S^{\circ}_{0,1}$ was also made.

As mentioned earlier in section 1:1 our intention has been focussed on the following subjects.

(A) The equilibria concerning condensation ion-molecule reactions in ethanol and the other thermodynamic quantities derived from equilibrium constants.

(B) Determination of the rate constants of these reactions.

(C) The confirmation of reaction (17) at high temperatures i.e. 350°C.

The equipment and techniques used for the investigation of above mentioned items are fully described in the second chapter (Chapter 2: Apparatus).

2. APPARATUS

2:1 The Requirements and Design of the Instrument

The instrument was designed to fulfill the requirements of our current research indicated below.

(a) Operation at high pressures of several torr in the ion source is to be achieved.

(b) The ionizing radiation source should be easy to pulse.

(c) Any gradual spreading effect of the ionizing radiation source in the vacuum and resulting contamination of the apparatus must be avoided.

(d) The mass analyzer should have a high transmission and thus great sensitivity.

(e) The mass analyzer itself should be compact and easy to mount.

(f) The cost of mass analyzer should be relatively low.

(g) Operation at high temperatures up to 400°C must be possible.

Requirement (a) was met by designing an ion source with small electron entrance and ion exit slits and thus with a low overall conductivity so as to allow maintenance of a large pressure differential between the ion source and the vacuum chamber containing the mass analyzer.

Requirements (b) and (c) could be satisfied by

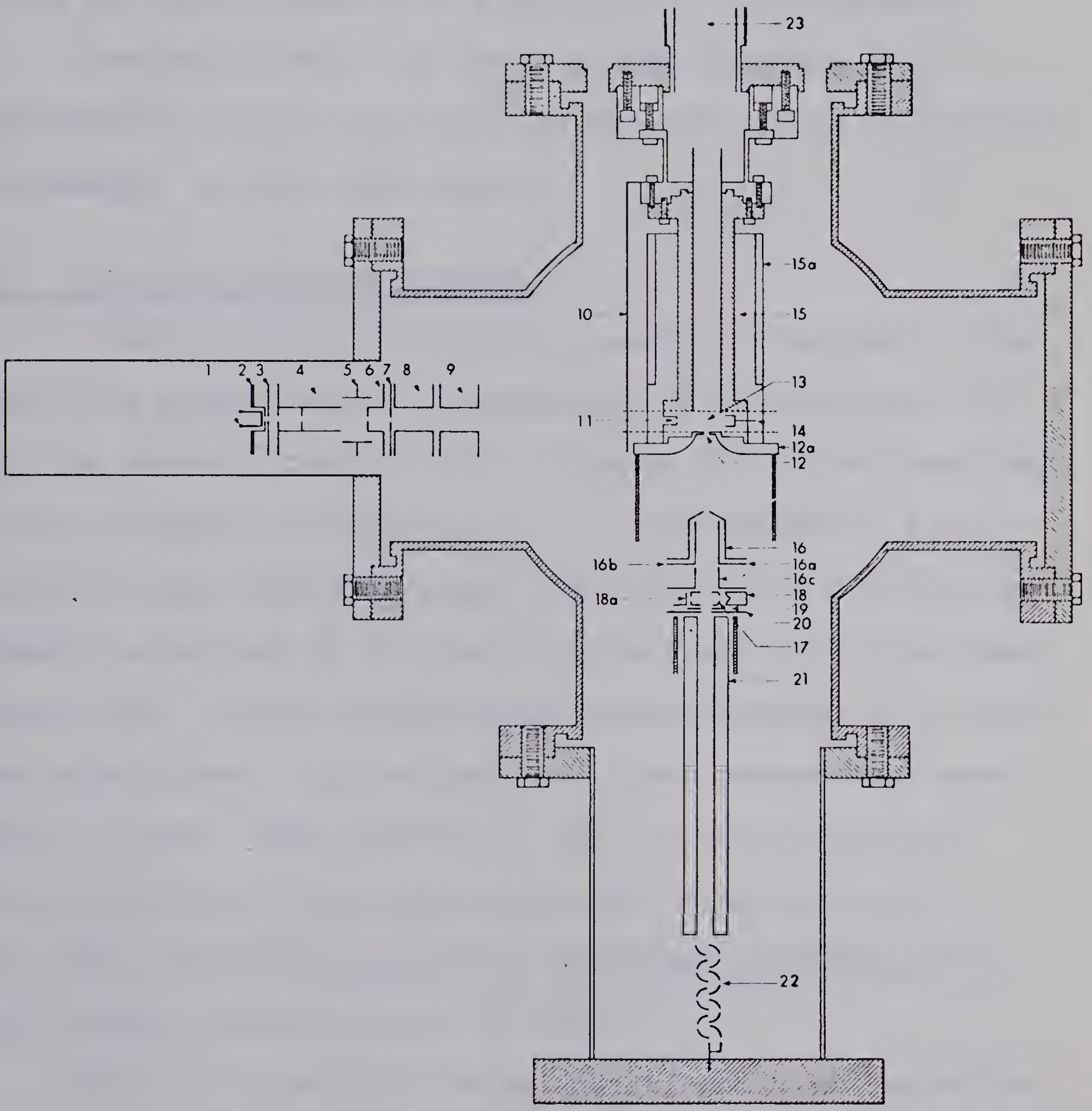

FIGURE 2:1 Apparatus; (1) - (9) electron gun; (10) - (15) ion source assembly; (16) - (20) ion acceleration assembly; (21) mass filter rods; (22) secondary electron multipliers; (23) gas inlet.

using an electron gun which has been able to produce a 3000 eV electron beam as the ionizing radiation.

The three requirements (d), (e), (f), could be fulfilled by the employment of a quadrupole mass analyzer.

The requirement (g) could be met by means of a replacement of the viton seals on the ion source of previous instruments by the gold seals.

2:2 The Gas Handling System.

This system was designed to serve two purposes, the sample gas supply and the preparation of gas mixtures for the ion source. The schematic drawing of the gas handling system is shown in Figure (2:2). The materials of construction were stainless steel and glass. The whole valve assembly consisted of ten large conductance stainless steel valves ((5), Varian ½-inch/viton sealed) mounted on a stainless steel frame. In the gas line other connections were made of glass. The pressure in the ion source and the glass manifold of the inlet system was measured by an Atlas MCT (Membrane Capacitance Torrmeter) manometer (7) which reads pressures up to 20 torr.

The gas handling system (plant) could be pumped by either a rough pumping system (1) or a clean pumping system (2).

The rough system (1) was used for removal of large amounts of gas. The clean system (2) was employed to dispose

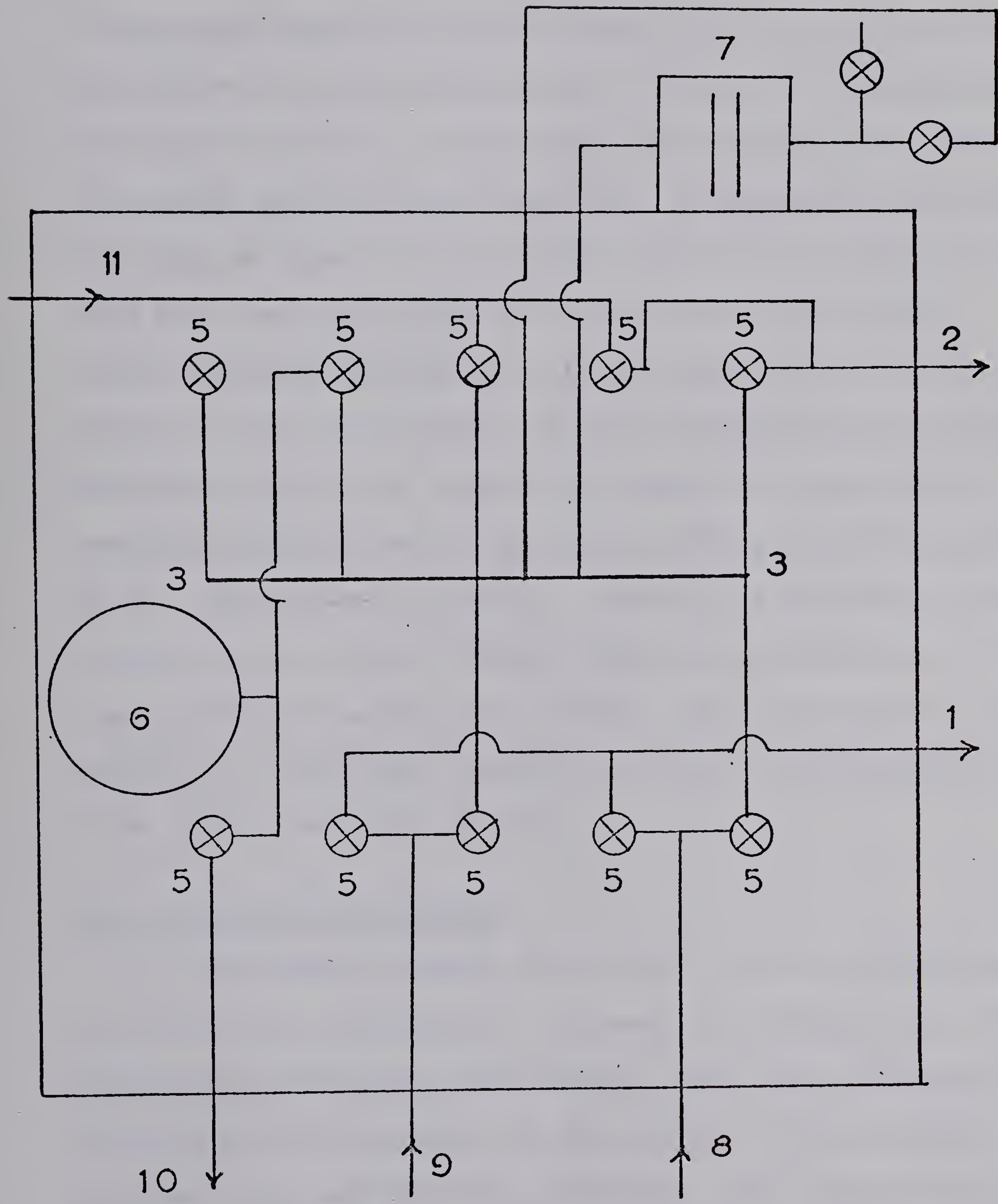

FIGURE 2:2: (1) rough system; (2) clean system; (3) glass manifold; (5) stainless steel valves; (6) bulb; (7) MCT; (8) sample inlet I; (9) sample inlet II; (10) cold finger.

of the last traces of gas and was used at all times when the system was maintained under vacuum. As a consequence, the impurity levels in the gas inlet system and in the ion source could be kept very low. A pressure differential due to flow of gas between the bulb (6) which was used for the preparation of gas mixtures and the ion source could be avoided by the stainless steel valves (5) placed in the line between the bulb and manifold, and the manifold and the ion source. By means of three spiral heating elements the baking out procedure could be applied up to temperatures of 150°C. Since this was made in consideration of matched thermal expansion coefficients of construction materials no breakage could be observed. The system as a whole was thermally isolated by an asbestos cover which was cubic in size.

2:3 The Vacuum Chamber

The vacuum chamber (Figure 2:1, (24)) was designed to contain the components, ion source, electron gun, and quadrupole filter and consisted of 75/8" O.D. stainless steel tube 9" in length. At the center of the chamber four 4½" O.D. and 1½" long stainless steel parts were welded mutually perpendicular into the chamber tube to provide and support mounting flanges. The first flange held the ion source assembly. The flange opposite this held the quadrupole and the flange at right angle

to these held the electron gun. The last flange was used as a spare. The chamber was connected to an N.R.C. (National Research Corporation) VHS-6, type No. 0184, 2400 liters per seccnd capacity diffusion pump through a water-cooled optical baffle. The pumping at the top of the baffle was stated to be 1050 l/sec (operating instructions, N.R.C. equipment division).

One of the ways to calculate the pumping speed (S) at the point which is in the immediate vicinity of the ion source is by means of the equation [30] given below.

$$S = \frac{S_p \cdot F_{tube}}{S_p + F_{tube}} \tag{21}$$

where S_p is the speed of the diffusion pump at the top of the baffle, and F_{tube} is the conductance of the vacuum chamber tube. Since the flow is molecular and the vacuum chamber tube has a circular cross-section, F_{tube} can be evaluated by the equation

$$F_{tube} = \frac{2}{3} \pi . \bar{v} \frac{r^3}{\ell} \tag{22}$$

where $\bar{v}$ is the average velocity of the gas molecules, r is the radius of the tube, and ℓ is the half length of the tube. By taking,

$\bar{v} = 4.0 \times 10^4$ cm/sec (air)

$r = 9.5$ cm

$\frac{1}{2}(\ell) = 11.4$ cm then

$$F_{tube} = \frac{2}{3} \times \pi \times 4.0 \times 10^{4} \times \frac{(9.5)^{3}}{11.4} = 6300 \text{ l/sec}$$

thus the pumping speed (S),

$$S = \frac{S_p \times F_{tube}}{S_p + F_{tube}} = \frac{1050 \times 6300}{1050 + 6300} = 863 \text{ l/sec}$$

2:4 The Ion Source

The ion source where the ionization by a high energy electron beam impact of the gases under investigation occurs is shown in Figure (2:3). It consisted of a 4¼" long non-magnetic stainless steel cylinder.

Two glass inlet tubes (23) (one inside the other) were sealed into the ion source mounting flange by means of a rubber o-ring to let the gas flow through.

On the lower left hand side a slit for the entrance of the electron beam was mounted (11). This slit was made by welding stainless steel razor blades to a circular bottom disc of a stainless steel cylinder which contained a hole 4.5 mm x 1.7 mm in size. The final size of the slit was 2 mm x 0.020 mm. At the other end of the cylinder a small flange was placed to mount the slit into the ion source.

On the lower right hand side (right across the electron entrance slit) the ionization chamber was plugged by a stainless steel flange which was welded on to a Kovar glass high resistance electrical feed through that

was connected (soldered) to a stainless steel cylindrical Faraday cup. The primary and secondary electrons could be collected by this arrangement , it is called an electron trap (14).

The ions left the ion source through a small slit (12) mounted at the bottom of the ion source. This slit was 1.6 mm x 0.020 mm in size and could be made by the welding of two stainless steel half circular razor blades onto a specially designed flange.

Both of these flanges (electron entrance, electron trap, ion exit) were mounted and sealed into the ion source by means of small screws and gold o-rings.

Below the ion source an electrostatic shield, which provided a boundary for the electric field between the ion source and the ion acceleration electrodes, was mounted. The shield was a thin wall cylinder slotted longitudinally so that the gas pumping speed was as high as possible, without deforming the electric field.

In front of the electron beam entrance slit the electron beam focus plate (10) was placed. This plate had a 12 mm diameter hole axial with the electron entrance slit. A mixture of phosphor, sodium silicate, and sodium chloride was applied to the plate to form a coating. The electron beam caused the phosphor to emit a green light so the beam could be seen and focussed. The sodium chloride was added to make the phosphor coating

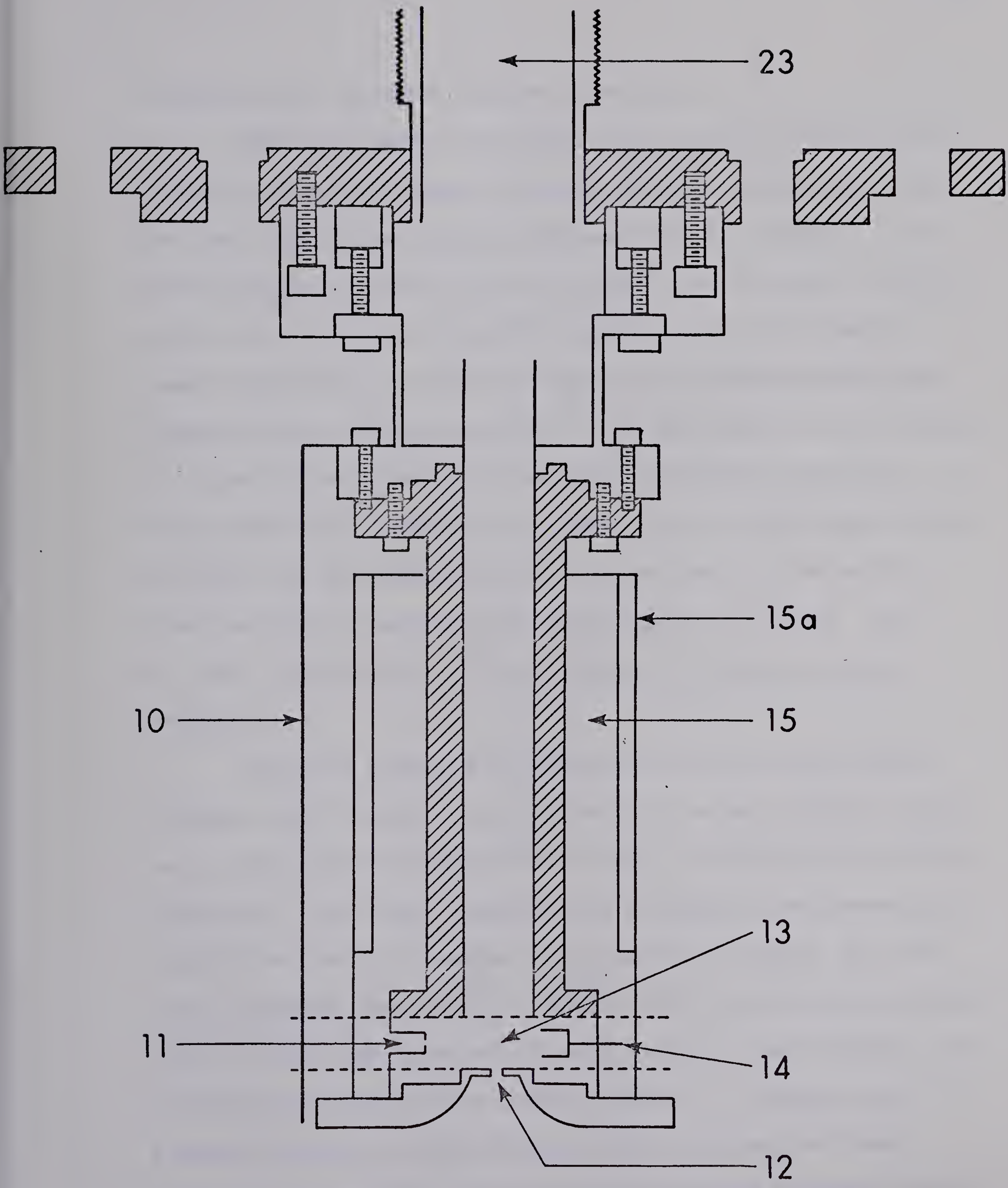

FIGURE 2:3 Ion Source; (10) electron beam focus plate; (11) electron entrance slit; (12) ion exit slits; (13) ionization region; (14) electron trap; (15) copper jackets; (23) gas inlet.

conductive to prevent surface charging.

The ion source was heated by a block heater placed in the grooves of copper jackets (15) each half cylindrical and 2 5/8" long which surround the ion source. The block heater was made from 28 gauge nichrome wire, spiral wound and insulated from the copper jackets by quartz tube insulators. Two iron constantan thermocouples were inserted into the ion source. One was close to the heaters so that it could be used for the temperature control. The second was inserted in a well close to the gas chamber so that the gas temperature could be read. The assumption was made that the gas temperature was the same as the temperature of the walls of the ion source chamber.

The ion source was mounted on one of the vacuum chamber port flanges by a cylindrical steel support which was electrically insulated by a disc of machinable ceramic material. The steel support was slotted to decrease heat conduction and its length was planned to adjust the distance between the mounting flange and the electron entrance slit so that the beam could pass through the central line of the main tube of the vacuum chamber. Ceramic was bolted directly to the flange which remained at room temperature and thus its temperature could be kept approximately the same.

There were twelve electrical feed throughs on the

flange. The glass gas inlet tubes were heated by nichrome wire heaters wrapped around the glass.

Calculations were made to evaluate the conduction of the ion source (F_s) as shown below

$$F_s = F_{ee} + F_{i.e} \tag{23}$$

where F_{ee} is the conduction of electron entrance slit, $F_{i.e}$ is the conduction of ion exit slit.

However, conduction of a slit (cc/sec) is given by

$$F = \frac{\bar{v}}{4} \times A$$

where A is the area of aperture (cm^2)

$$\bar{v} = 40000 \text{ cm/sec (for air), then}$$

$$F_{ee} = \frac{40000}{4} \times 0.2 \times 0.002 \simeq 4 \text{ cc/sec}$$

$$F_{i.e} = \frac{40000}{4} \times 0.16 \times 0.002 = 3.2 \text{ cc/sec}$$

$$F_s = 4 + 3.2 = 7.2 \text{ cc/sec}$$

2:5 The Electron Gun

The electron gun which produces a high energy electron beam is shown in Figure (2:4). It consisted of a tungsten ribbon filament to emit the electrons (thermoionic emission) and a series of non-magnetic stainless steel focussing plates (electrostatic focussing). The operational scheme of the electron gun can be outlined

as follows:

The electrons were emitted from an electrically heated tungsten ribbon (1) in the figure (0.508 cm x 0.076 cm) in size which was kept at very low potentials such as -2750 V to -2850 V.

They were then drawn out and extracted by draw out (2) and extractor (3) plates. The draw out plate was pulsed to approximately (+40 V) with respect to the potential at the center of the tungsten ribbon. On the other hand the extractor was maintained at the same potential that the center of the ribbon had.

The electrons just passed the extractor were accelerated and focussed by the focussing plates (5). These plates had the maximum positive potential (or approximately +550 V) with respect to the center of the ribbon among all plates of the focussing assembly.

Then they passed through the second acceleration region (6) and were collimated by the collimator plate (7).

The final step in the electron beam path was the deflection which was accomplished by at first Y directional deflection plates (8) and secondly X directional deflection plates (9). The positive potentials (with respect to the center of the ribbon) on these deflection plates were very low (6, 10 V)

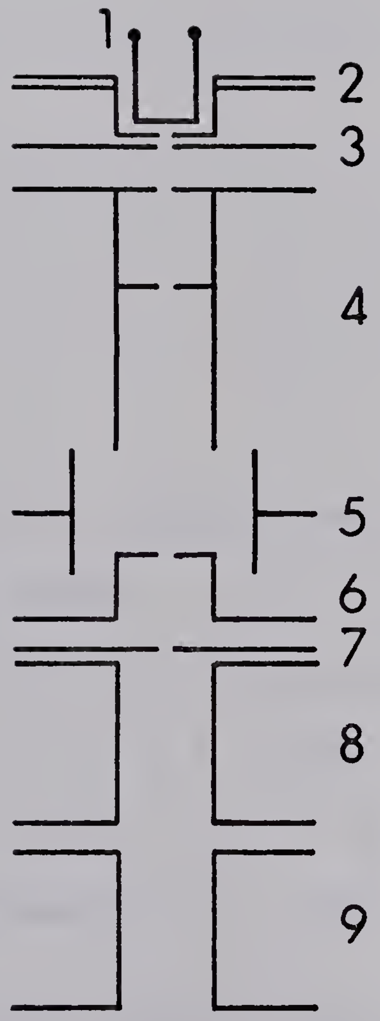

FIGURE 2:4 Electron Gun; (1) filament; (2) drawout plate; (3) extractor; (4) and (5) focussing; (6) accelerator; (7) collimator; (8) Y deflection; (9) X deflection.

Typical Potential Settings

(with respect to the center of filament)

Filament	3.8 Amps.
Drawout	+40 V
Extractor	0 V
Focus	550 V
X_2	10 V
Y_2	6 V

With these typical potential settings the following measurements were made

Spot size = 2 mm (diameter)

Emission current = 100 μa

Case current = 5 μa

Electron trap current $\simeq 10^{-8}$ amp

A voltage divider powered by a high voltage power supply was designed and used to adjust the potentials on the plates for optimum focussing.

The sizes of the central holes of the above-mentioned plates and a table of typical potential settings of the plates are given below.

Hole Dimensions

Drawout	0.076 cm
Extractor	0.193 cm
Accell.	0.233 cm
Collim.	0.317 cm

The transmission calculated from this data was

$$\text{Transmission} = \frac{\text{Case Current}}{\text{Emission Current}}$$

$$= \frac{5\ \mu a}{100\ \mu a} = 0.05$$

2:6 Ion Acceleration, Gating, and Travel Time

The ion acceleration and gating system which consisted of a series of electrodes is shown in Figure (2:5).

Ions leaving the high pressure ion exit (12) were accelerated by the negative potential of the quadrupole entrance cone (16). This cone was mounted upon the existing quadrupole mass spectrometer ion source plates (17) to (20) and contained two half-cylindrical plates (16a) and (16b) inside of it. These plates were deflection plates. The deflection and gating could be accomplished by keeping the electrode (16b) at the cone potential and applying a negative pulse of the same amplitude to the other deflection plate (16a). The focussing plate (19) and all other electrodes (16c) to (20) were kept at ground potential while the experiments were on.

The case and trap potentials of the main ion source were maintained at the same, small, positive value in order to obtain maximum signal on the high

mass range of the analyzer.

The typical potential settings for the electrodes are shown in the table below.

Ion Acceleration Potentials

Ion Exit Slit (12)	+ 7.5 V
Ion Source Case (13)	+ 7.5 V
Electron trap (14)	+ 7.5 V
Cone (16)	- 67.5 V
Deflection Plate (16a)	- 67.5 V (gate open)
Deflection Plate (16a)	0 V (gate closed)
Delfection Plate (16b)	- 67.5
(16c)	0
17	0
18	0
Focussing Plate (19)	0
20	0

The travel time of an ion from the ion source to the point at which the ion "gate" potential was applied could be calculated on the basis of two assumptions (a) and (b).

(a) The ions were accelerated across a
f
uniform yield between the ion exit
slit cone (12) and the quadrupole entrance
cone (16).

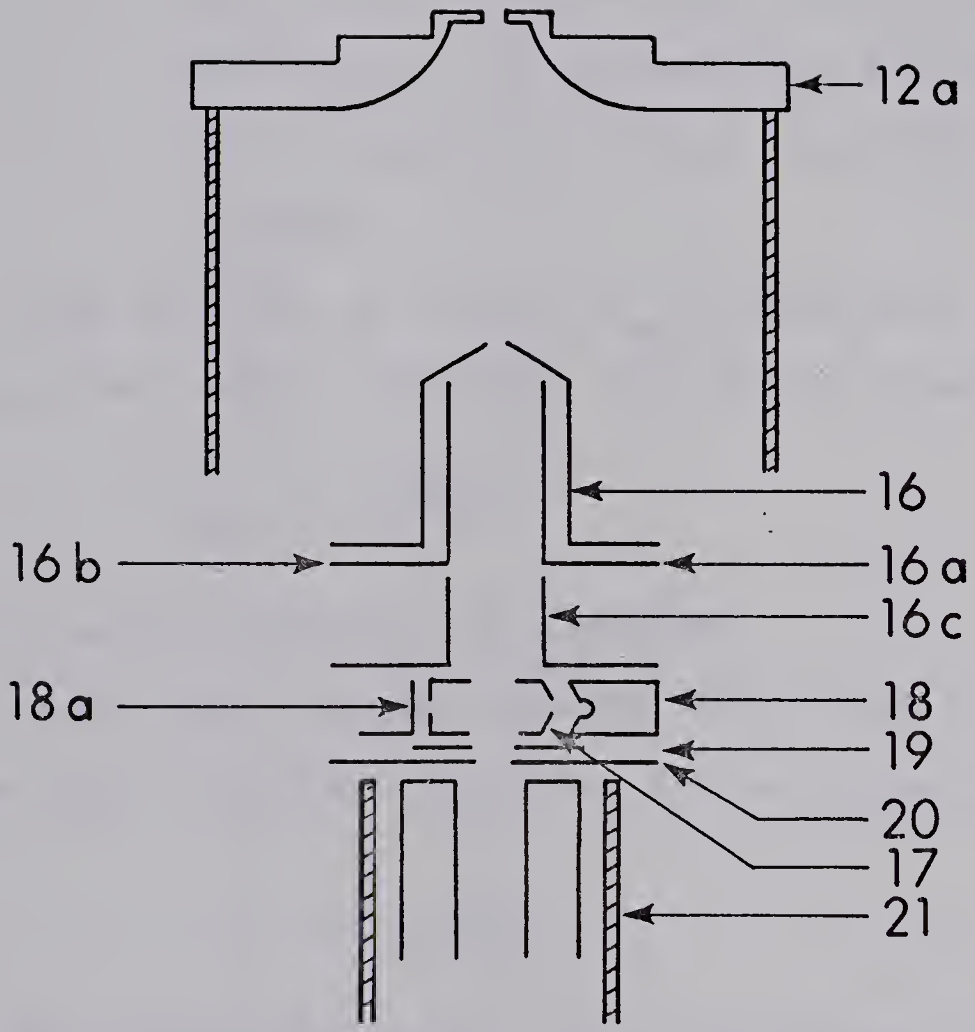

FIGURE 2:5 Ion Acceleration; (16) quadrupole entrance cone; (17-20) existing quadrupole mass spectrometer ion source plates; (16a) and (16b) deflection plates; (16c) electrode; (21) alumina tubing.

(b) Then they travelled to the ion gate through the cone at a constant velocity. In other words there was no acceleration in the region between the entrance of the ion entrance cone and the ion gate plate where they were stopped.

The velocity of an ion (V_{acc}) with mass (m) in a uniform field with a potential V is known to be [32]

$$V_{acc} = \left(\frac{2\ eV}{m}\right)^{\frac{1}{2}} \qquad (24)$$

where e is the charge of an electron.

Since the average velocity ($\bar{v}$) is the half velocity of the final velocity (V_{acc}) in the acceleration region

$$\bar{v} = \frac{1}{2} V_{acc} \qquad (25)$$

thus, the crossing time for the acceleration region (t_{acc}) is

$$t_{acc} = \frac{\text{distance between the cones}}{\bar{v}} = 2\,\frac{S_{acc}}{V_{acc}} \qquad (26)$$

Because of the second assumption (b) made above the crossing time in the constant velocity region (t_{cv}) is

$$t_{cv} = \frac{S_{cv}}{V_{acc}} \qquad (27)$$

The total flight time (t_f) should be

TABLE 2:1

Table of Calculated Flight Times

Mass (m)	$\sqrt{m}$	$t_f(V = -225\ V)$	$t_f(-67.5\ V)$
10	3.17	1.29×10^{-6} sec	2.35×10^{-6} sec
15	3.87	1.57	2.88
20	4.46	1.82	3.31
25	5.00	2.03	3.71
30	5.47	2.22	4.06
40	6.32	2.57	4.69
50	7.07	2.87	5.25
60	7.74	3.15	5.75
70	8.36	3.40	6.21
80	8.95	3.64	6.65
90	9.50	3.87	7.05
100	10.00	4.07	9.43
120	10.95	4.46	8.14
140	11.84	4.82	8.79
160	12.66	5.15	9.40
180	13.42	5.46	9.98
200	14.14	5.75	10.50

where $S_{acc} = 35$ mm and $S_{cv} = 15$ mm.

$$t_f = t_{acc} + t_{cv} \tag{28}$$

$$t_f = (2\ S_{acc} + S_{cv}) \left(\frac{m}{2\ eV} \right)^{\frac{1}{2}} \tag{29}$$

Table 2:1 lists the calculated flight times of ions of different mass. In this table the evaluations have been made for two different acceleration potentials (V_1 = -225 v and V_2 = -67.5 v) and actual machine measurements (S_{acc} = 35 mm and S_{cv} = 15 mm) were used.

2:7 Pulse Circuits

The schematic diagram of the pulse generators is shown in Figure 2:6. The wave forms are shown in Figure 2:7. The first pulse generator was employed to generate the pulse of width (Δt_e) applied to the electron gun drawout plate. Thus the electron was on for the time Δt_e (generally 10 μsec). The synchronization signal from the first generator was fed into the oscilloscope (Hewlett Packard 130-CX) of the mass analyzer and into the generator (2). The second generator was used to vary the delay time (t"). The output of the second generator (actually the delayed synchronization pulse) was used to trigger the third generator (Datapulse Model 101) which produced the ion gate pulse of width (Δt_i).

The generators 1,2 were made by the electronic

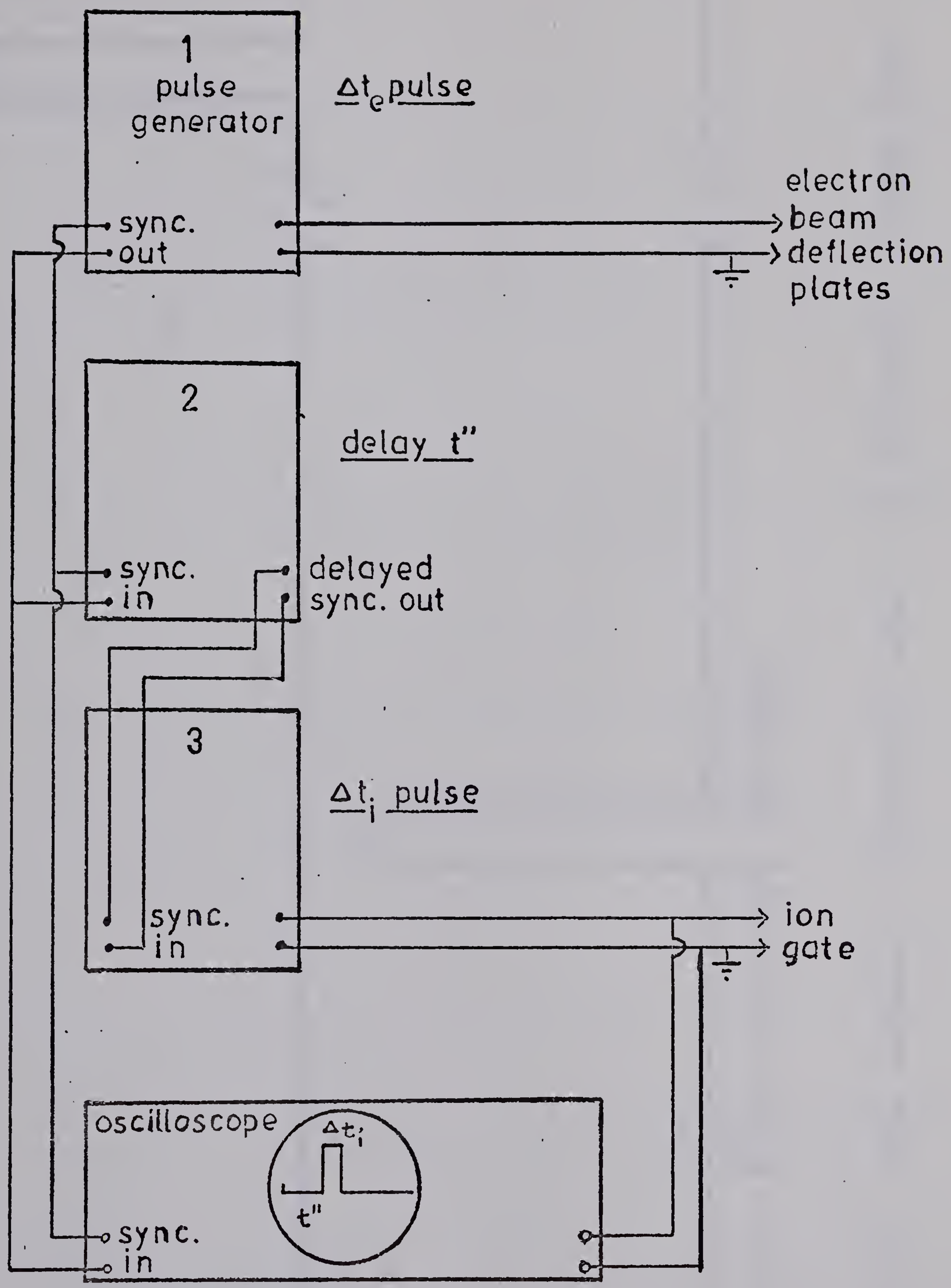

Figure 2:6 Pulse generation circuit

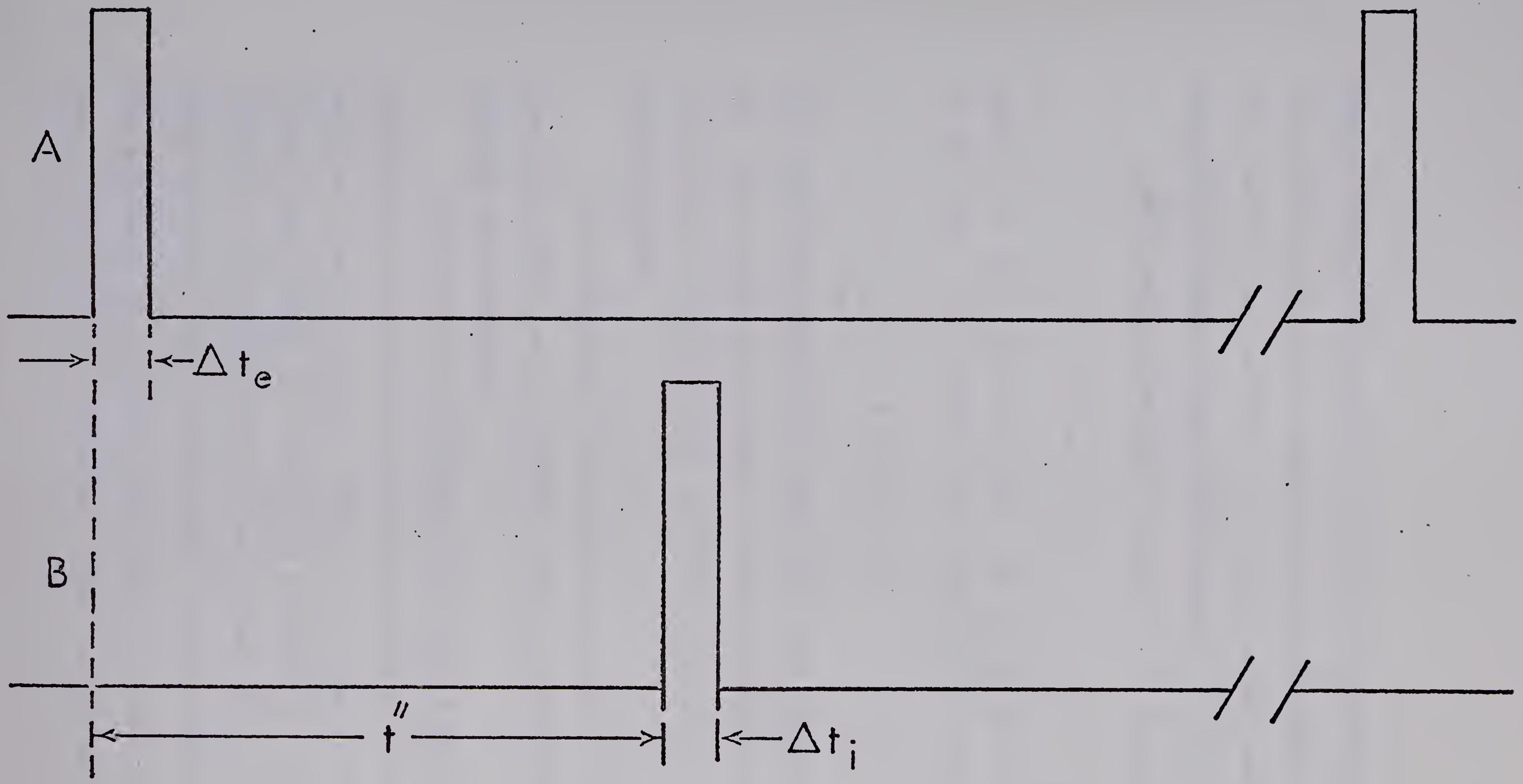

Figure 2:7 Pulse sequence. Δt_e electric pulse, Δt_i ion pulse, t'' delay pulse .

shop of this institution. The delay time which was the time between the pulse applied to the drawout plate of the electron gun and the ion gating pulse, was measured visually by means of the oscilloscope.

This delay time (t") is given by the equation

$$t'' = t + t_f \qquad (30)$$

where t is the reaction time, and t_f is the flight time of the ions. By solving this equation for (t),

$$t = t'' - t_f \qquad (31)$$

the conclusion should be drawn that the reaction time is the time spent by the ions in the ion source and in the time interval between the electron beam and the ion gating pulses.

The technique of ion gating to set the reaction time was chosen as it allowed the mass spectrometer to operate continuously.

The period of electron beam pulses was selected sufficiently long (2000 μsec) to assure the complete decay of the ion current during this time interval.[33] On the other hand, it should be pointed out that the operation with electron and ion pulses which are so short compared with the interval between pulses requires the presence of a large ionic signal in the continuous mode of operation. Therefore, there would be significant

loss in signal and the loss factor would be varied from 10^2 to 10^5 depending on the length of the reaction time,

2:8 The Quadrupole Mass Filter and the Detection System

(A) Theory of the Quadrupole

The quadrupole mass filter principle was first described almost simultaneously by Post and Henrich [34], and by Paul and Steinwedel.[35] It consists of four rods of hyperbolic cross section. The quadrupole field is created by the application of a D.C. voltage (u) and a superimposed rf voltage (V_o.Cos wt) on these four electrodes. Opposite pairs of electrodes are electrically connected. The arrangement is shown in Figure 2:8. As a result the positive pair of electrodes has a potential $+(u + V_o.\text{Cos } wt)$ and the negative pair a potential $-(u + V_o.\text{Cos } wt)$. The potential generated by cylindrical electrodes at any point of quadrupole field is approximated by the equation,

$$V = (u + V_o.\text{Cos } wt) \frac{(x^2 - y^2)}{r_o^2} \qquad (32)$$

where x is the dimensional value on the axis of positive rods, y is the dimensional value on the axis of negative rods, $2r_o$ is the electrode spacing, t is time, and w is the operating frequency of the rf voltage.

The differential equations relating to the electrical forces and acceleration of the ions are given

below,

$$\frac{m}{e}\frac{d^2x}{dt^2} + 2(u + V_o.\text{Cos } wt)\frac{x}{r_o^2} = 0 \quad (33)$$

$$\frac{m}{e}\frac{d^2y}{dt^2} - 2(u + V_o.\text{Cos } wt)\frac{y}{r_o^2} = 0 \quad (34)$$

$$\frac{m}{e}\frac{d^2z}{dt^2} = 0 \quad (35)$$

The first two equations can be rewritten in the canonical form (Mathieu equations) as follows

$$x'' + (a + 2q\text{ Cos } 2\delta)x = 0 \quad (36)$$

$$y'' - (a + 2q\text{ Cos } 2\delta)y = 0 \quad (37)$$

where the primes denote differentiation with respect to δ and

$$wt = 2\delta \quad (38)$$

$$a = \frac{8eu}{mr_o^2w^2} \quad (39)$$

$$q = \frac{4eV}{mr_o^2w^2} \quad (40)$$

The solutions of these Mathieu equations designate oscillations performed by an ion in the x and y directions respectively. At the same time the ion travels with constant velocity and consequently zero acceleration along the z axis. For certain values of a and q the oscillations

are stable, in other words the amplitude remains finite and less than electrode spacing ($2r_o$) at any time t. But for the other values of a and q the oscillations are unstable and the amplitudes are greater than electrode spacing and approach infinity exponentially.

Conditions under which ions achieve a stable trajectory in the x and y directions can be determined by reference to a "stability diagram".

The stability diagram Figure (2:9) is a plot of the parameters a and q which graphically demonstrates stable solutions of the Mathieu equations. If the ratio a/q is kept constant the representative points for different ionic masses will fall on a straight line passing through the origin of the stability diagram. For masses like m_1 where the point falls inside the stability region, ions continue their travel on an oscillatory path through the quadrupole field; for other masses such as m_2 the ions are lost be lateral deflection. Thus a mass separation may be achieved. If a and q are varied while the a/q ratio is maintained constant the range of masses which continue through the field is also varied. Consequently the scanning could be done by varying u and V_o maintaining a constant ratio or by varying the operating frequency w.

Resolution is defined as $M/\Delta M$ where M is the mass-

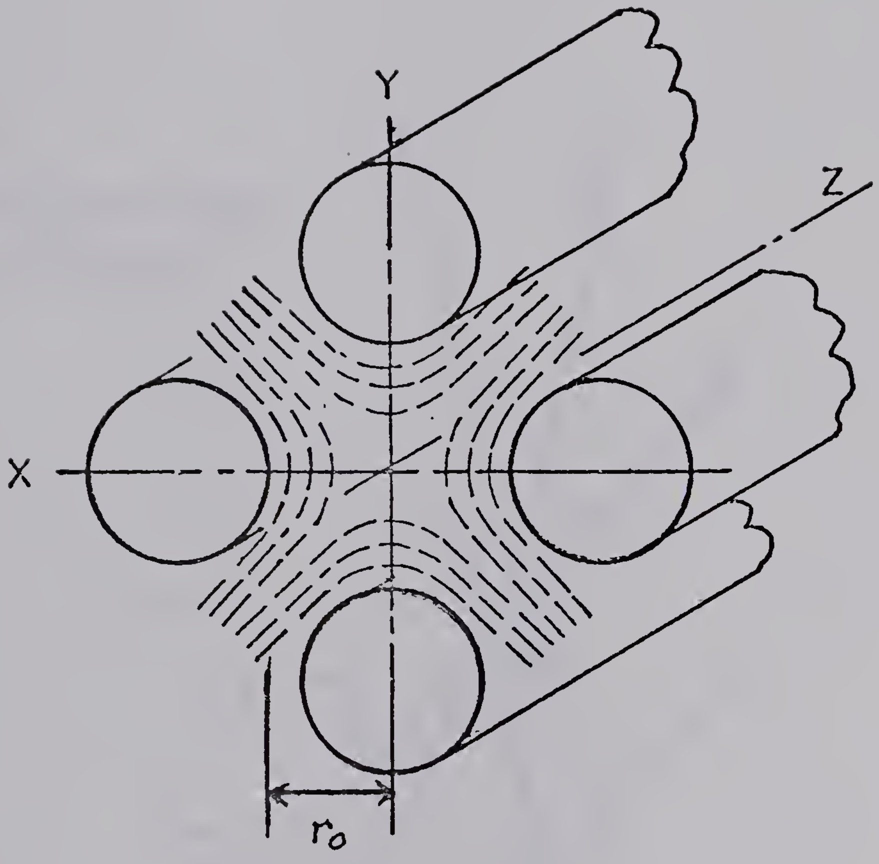

FIGURE 2:8

DRAWING SHOWING QUADRUPOLE ROD STRUCTURE WITH THE HYPERBOLIC FIELD LINES. "X" AND "Y" RODS ARE SHOWN. THE "Z" AXIS IS THE AXIS OF THE ROD STRUCTURE.

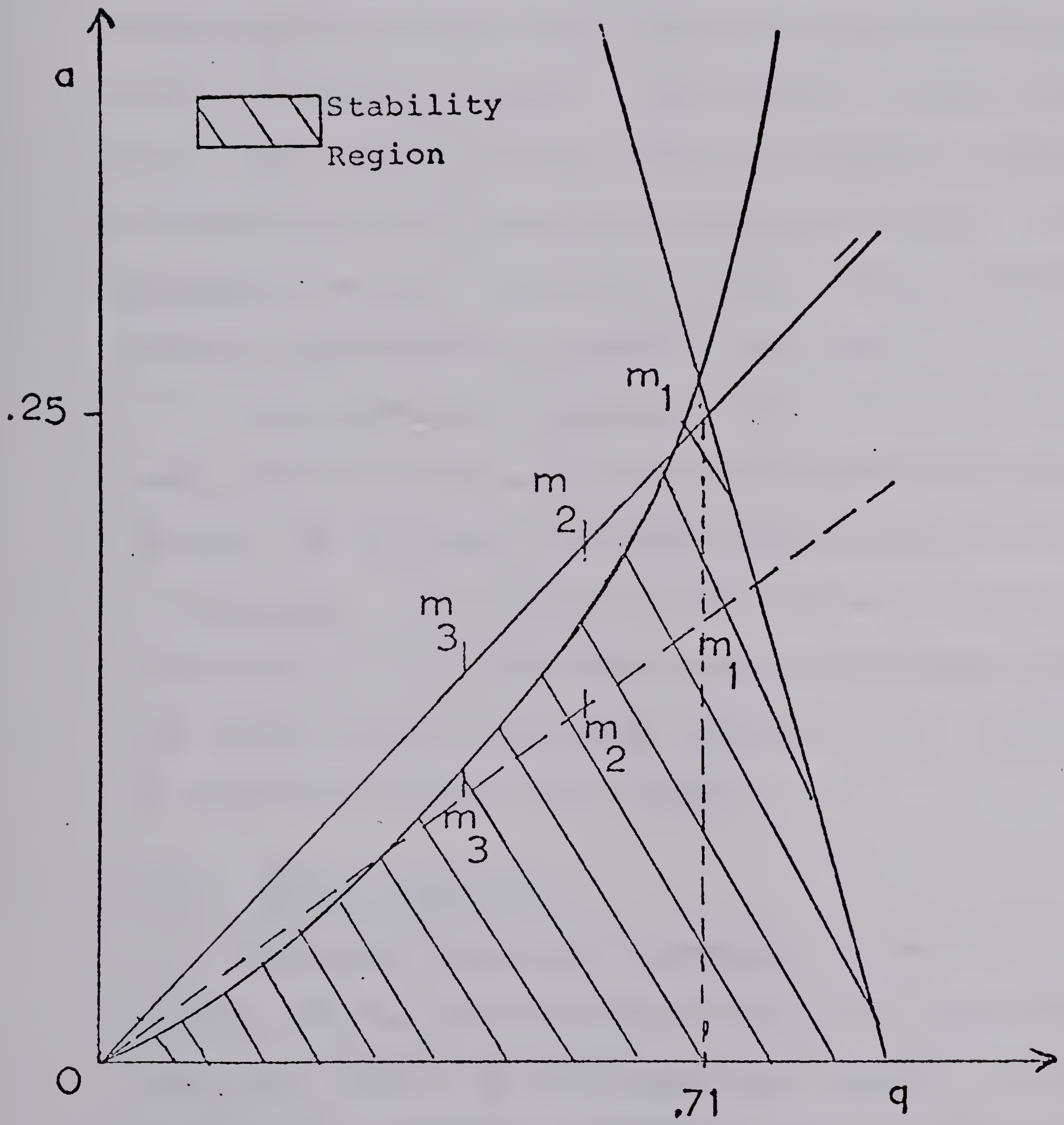

FIGURE 2:9 Stability Diagram

to-charge ratio of the ion of interest and ΔM is the width of the mass peak in amu at half peak height. ΔM can be decreased and therefore the resolution increased by increasing u/V_o voltage ratio. This will cause the working point of the mass filter to approach the apex of the stability diagram. The region in which ions of a given mass-to-charge ratio can achieve stable trajectories will become more narrow resulting in ΔM becoming smaller. Resolution then increases and theoretically approaches infinity at the apex.

The practical requirement for an actual quadrupole mass filter is that an ion should be able to travel through the analyzer of finite length without striking an electrode. An important consequence of this practical requirement is that the mass resolution becomes dependent on the lateral positions and the radial velocities of the ions entering the analyzer.

(B) RF/DC Generator.

The RF/DC generator provides the RF voltage (V_o. Cos wt) and the DC voltage (u) which is applied to the quadrupole rods. It has three mass ranges, 1-50 amu (low range), 10-250 amu (medium range), and 100-750 amu (high range). The mass number which places at the center of the displayed spectrum is selected by the mass number control. The calibration data and plots of mass number

versus (m/e) ratio are given in Table 2:2 and Figure 2:10 for all three ranges. Total ionization measurement is accomplished via a switch which removes the DC voltage from the mass filter rods. This feature allows all species of ions to traverse the mass filter without any filtering action.

(C) Mass Filter

The mass filter consists of four 5½" long nonmagnetic stainless steel cylindrical rods spaced in a rectangular array by precision high alumina ceramics. The arrangement of filter rods and the fields within the rod system are shown in Figure (2:8).

(D) Detection System.

The ion signals in the apparatus were detected by a fourteen stage, copper-beryllium secondary electron multiplier (SEM). The advantage of the electron multiplier is its capability of amplifying the ion current signal by a factor between 10^3 and 10^6. The disadvantage of the (SEM) is its variable gain with time. Moreover, SEM has another disadvantage in that all ions cannot be detected with equal efficiency.

The total number of electrons ejected from the first dynode depends upon its velocity and its chemical composition. During acceleration the ions all gain the same energies and thus their velocities are inversely

TABLE 2:2

Mass Number Reading

m/e	Low	Medium	High
14	127		
18	175		
19	184		
28	295		
32	345		
40	441		
47		105	18
71		178	41
83		214	53
94		250	63
106		287	74
120		331	88
143		402	110
153		434	120
155		440	122
190		544	159
223		636	192
225		642	494
260			231

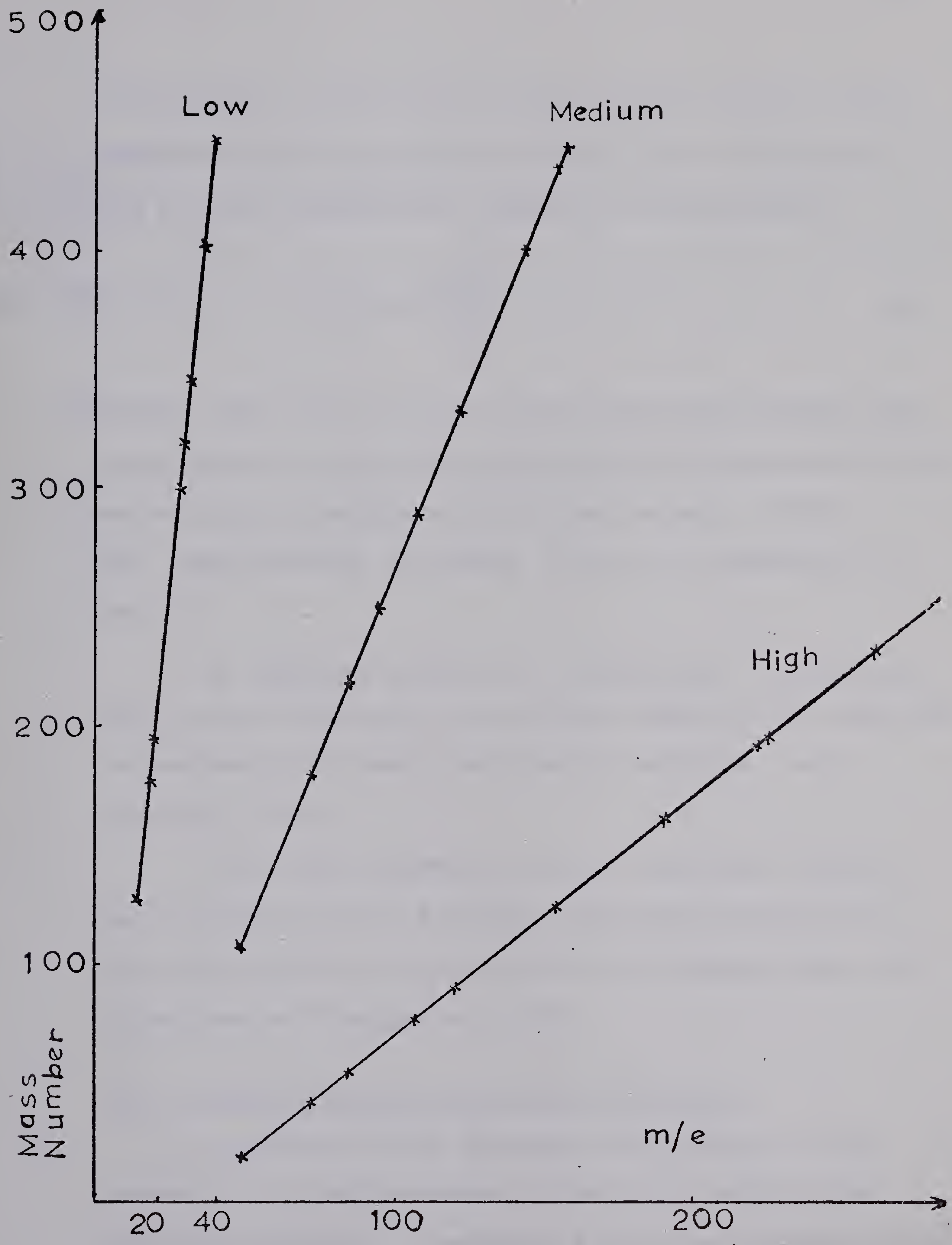

FIGURE 2:10; Mass Number Calibration

proportional to the square root of their masses. The relative electron currents for two ions of masses m_1 and m_2 will therefore be related by the equation

$$\frac{I_1}{I_2} = \sqrt{\frac{m_2}{m_1}} \qquad (41)$$

On the other hand, it is relevant that poly-atomic ions break apart on collision with the first dynode and behave as a group of particles of the same energy. Thus the amplification increases with the complexity of the ion.

If greater sensitivity limits must be achieved as it is in the case of this study, SEM must be connected to another high speed electrometer amplifier (e.g. Keithley 416X).

The probe assembly, and the electronic consule were manufactured by Finnigan Instruments Corporation and distributed by Granville-Phillips Company under the trade name of "Spectrascan 750".

(E) Electron Multiplier Gain Calibration

In order to make precise measurements of ion currents it is advantageous to know the gain of the electron multiplier. Because of the time dependent gain of the electron multiplier the gain measurements must be performed periodically. Calibration of the gain of

"Spectrascan 75Q" could be easily done by measuring the current out of the electron multiplier in normal operation (I_E), then measuring the current to the first dynode (I_F) and dividing I_E by I_F. Table 2:3 shows the I_E, I_F measurements and corresponding calculated gains.

(April 11, 1969).

TABLE 2:3

Ion	m/e	Mass Range	Mass No	I_E	I_F	Gain = I_E/I_F
He^+	4	Low	15.5	3.57×10^{-7}	1.9×10^{-11}	1.88×10^{4}
N^+	14	Low		9.18×10^{-8}	5.39×10^{-12}	1.7×10^{4}
O^+	16	Low		1.75×10^{-8}	1.33×10^{-12}	1.31×10^{4}
H_2O^+	18	Low		7.93×10^{-9}	6.26×10^{-13}	1.27×10^{4}
Ne^+	20	Low		5.17×10^{-7}	2.85×10^{-11}	1.81×10^{4}
N_2^+	28	Low		6.84×10^{-7}	3.55×10^{-11}	1.93×10^{4}
O_2^+	32	Low		6.55×10^{-8}	4.03×10^{-12}	1.63×10^{4}
Ar^+	40	Low		1.33×10^{-6}	5.46×10^{-11}	2.43×10^{4}
Kr^+	84	Medium		3.4×10^{-7}	2.22×10^{-11}	1.53×10^{4}
Kr^+	86	Medium		9.0×10^{-8}	6.6×10^{-12}	1.36×10^{4}
Xe^+	129	Medium		3.83×10^{-8}	1.85×10^{-12}	2.07×10^{4}
Xe^+	132	Medium		3.66×10^{-8}	1.30×10^{-12}	2.81×10^{4}
$(EtOH)_3H^+$	*139*	*High*		*207×10^{-8}*	*42×10^{-11}*	*4.93×10^{3}*
$(EtOH)_4H^+$	*185*	*High*		*262×10^{-7}*	*624×10^{-11}*	*4.1×10^{3}*
$(EtOH_5H^+$	*231*	*High*		*190×10^{-7}*	*456×10^{-11}*	*4.16×10^{3}*
$(EtOH)_6H^+$	*277*	*High*		*107×10^{-8}*	*26×10^{-11}*	*4.11×10^{3}*

Italic numbers represent the measurements made on June 5, 1969

3: RESULTS AND DISCUSSION

3:1 The Ions Detected and Reactions.

The ions which are detected under same typical conditions (1-2 torr ethanol pressure and 300°K) and the reactions involved in their formation are shown in Table (3:1).

The ion intensity time dependence of one typical run is shown in Fig. 3:1. These results were obtained with the electron beam pulsing and ion gate detection technique described in the experimental part. In order to correct for the decrease of total ion intensity after the electron pulse a normalization procedure was applied. This procedure consists of two succeeding parts. Firstly, one calculates the total ion current for the time (t) by summing individual ion currents at the time (t). Secondly, one evaluates the normalized ion intensities by dividing the individual ion currents by the total current both at the time (t). Previous work [33] in this laboratory using the above procedure had shown that considerable time is required if the calculations are performed manually with a desk calculator. Therefore it was considered useful to develop a program for the I.B.M. FORTRAN 360H system. A copy of the program is attached in the appendix.

As seen from Fig. 3:1 the normalized intensities of the ions $(C_2H_5OH)_3H^+$ became constant after considerably less

TABLE 3:1

The Detected Ions and Reactions in Ethanol

Ion	m/e	Reaction	Reaction No
$C_2H_5OH^+$	46	$C_2H_5OH + e^- \rightarrow C_2H_5OH^+ + 2e^-$	1
$C_2H_5OH_2^+$	47	$C_2H_5OH^- + C_2H_5OH \rightarrow C_2H_5OH_2^+ + C_2H_5O$	2
$(C_2H_5OH)_2H^+$	93	$(C_2H_5OH)_{n-1}H^+ + C_2H_5OH \rightleftarrows (C_2H_5OH)_nH^+$ (for n = 1....7)	3
$(C_2H_5OH)_3H^+$	139		4
$(C_2H_5OH)_4H^+$	185		5
$(C_2H_5OH)_5H^+$	231		6
$(C_2H_5OH)_6H^+$	277		7
$(C_2H_5OH)_7H^+$	323		8

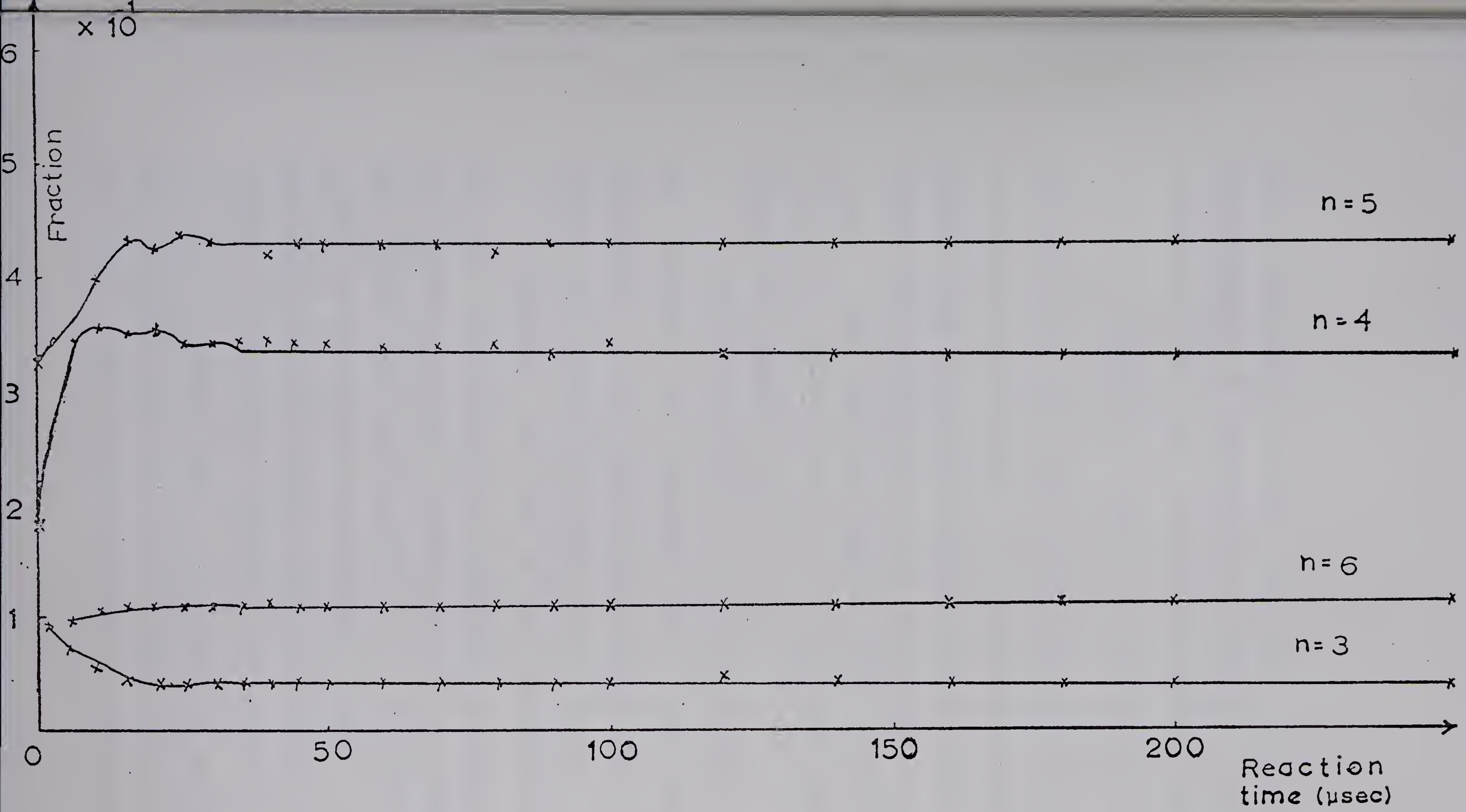

FIGURE (3:1)

The Normalized Ion Intensity - Time Curves

than 50 μsec reaction time. This must be due to the establishment of clustering equilibrium. Previous work on the kinetics of the clustering reactions has provided

$$H^+(H_2O)_{n-1} + H_2O \rightleftarrows H^+(H_2O)_n$$

rate constants which allow one to estimate the time required to reach the equilibrium. It can be shown that the water system, under conditions similar to those used in the present alcohol experiments, would reach equilibrium in less than 10 μsec. Thus the above results are in line with what could be expected since the kinetics of the water and ethanol systems are probably quite similar.

Since equilibrium is established within a very short time relative to the residence time of the average ion, the measurement of the equilibrium constant does not really require any electron pulsing and ion gating.

Therefore, the rest of the experiments which dealt with the determination of clustering equilibria were done with constant electron irradiation and ion detection. In fact, under these conditions the ion intensity is much higher and the over-all operation is easier. A somewhat more sophisticated technique which also gives relatively higher intensities but supresses the detection of ions with very short reaction times is described as follows. The electron beam is pulsed for a duration of about 50 μsec with a period of 2 msec. The ion detection gate is kept closed for

about 100 μsec and then opened til the next electron pulse. This technique was tried but found to be not as reliable as the constant irradiation procedure due to the stray electrons from the electron gun. These stray electrons produced ionization outside of the ion source both when the electron beam was entering into the electron entrance slit and when the beam was deflected.

3:2 The Equilibrium Constants.

(A) Early Results

Some representative equilibrium constants as a function of ethanol pressure at room temperature (∿ 30°C) are shown in Figure (3:2). As can be seen in Figure (3:2), the K_p values were dependent on the pressure. In fact, in all cases the K_p values decreased with increasing pressure. Because of this pressure dependent behaviour of the equilibrium constants it was found necessary to check the apparatus with a known system. The clustering system of water

$$H^+(H_2O)_{n-1} + H_2O \rightleftarrows H.^+(H_2O)_n$$

was selected since its behaviour is well known from the previous experiments in this laboratory.[36] The equilibrium constants determined with the present apparatus showed a pressure dependence similar to that observed with ethanol. Obviously, some conditions in the present apparatus did not allow the proper measurement of equilibrium ion

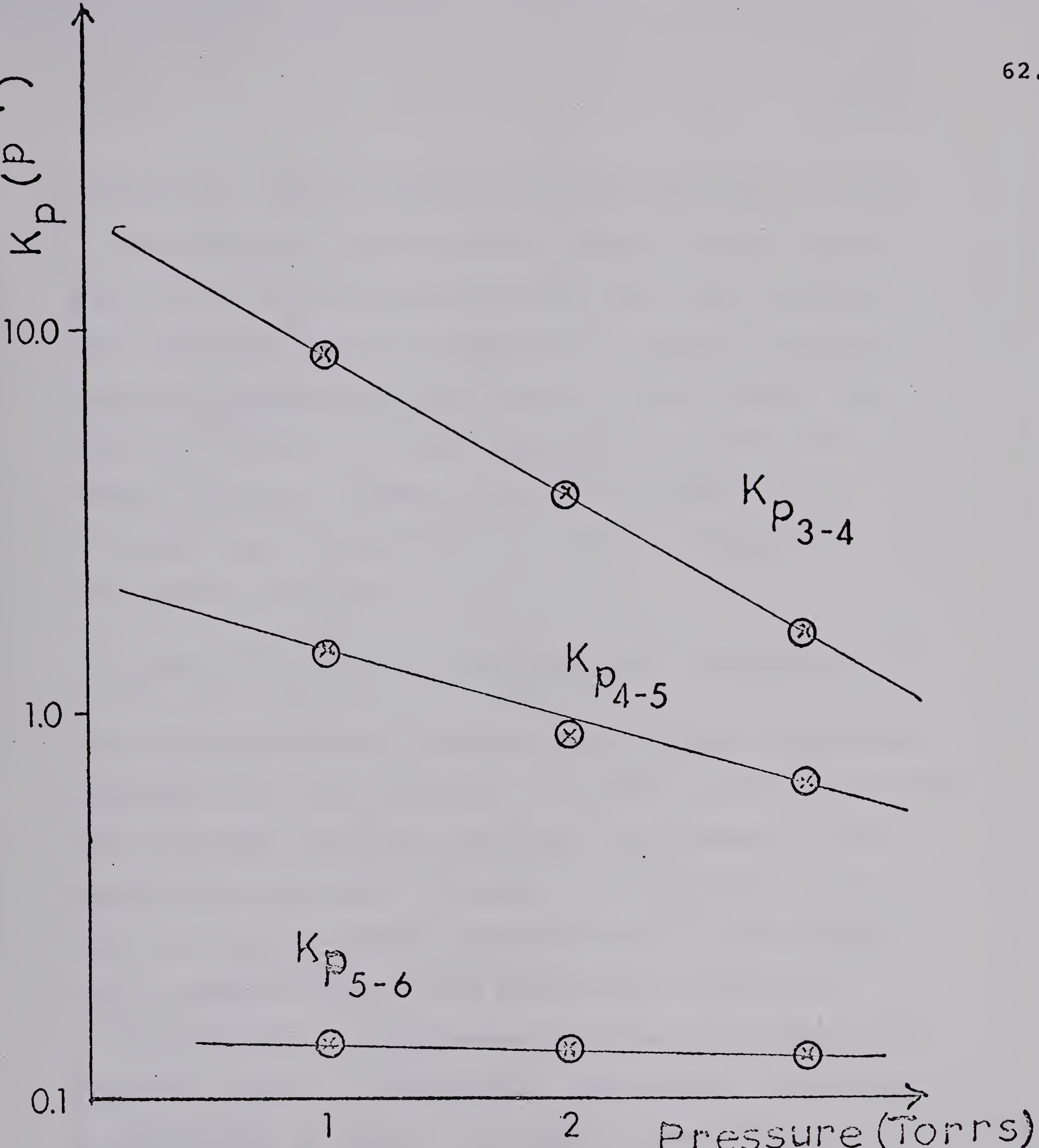

FIGURE (3:2)

The Equilibrium Constants of Ethanol as a Function of Pressure.

intensities. After considerable experimentation it could be shown that the pressure in the region outside the ion exit slit of the ion source was too high. The clustered ions $(C_2H_5OH)_nH^+$ after exiting the ion source and being partially accelerated by the electric field between the ion source and the cone electrode were colliding with ethanol molecules. These collisions involving ions of higher than thermal velocity lead to stripping reactions of the type:

$$(C_2H_5OH)_nH^+ \text{ (fast)} + M \rightarrow (C_2H_5OH)_{n-x}H^+ + x(C_2H_5OH) + M$$

The collision partner is indicated by M since any molecule can lead to the above reaction. In order to avoid the stripping collisions one has to decrease the pressure of the escaping gas molecules. The most efficient way to do that is to narrow the ion exit slit width. The original slit of dimensions 16 x 2000 microns was reduced to 7 x 2000 microns. Experiments were then made again with the water system. Considerable improvement was observed as illustrated in Figure (3:3) which shows the results for $K_{5,6}$ with the new and old slit. The equilibrium constant with the new slit remains constant with pressure for a longer pressure interval. It should be also noted that both curves extrapolate at low pressures to the published value determined earlier in these laboratories.[36]

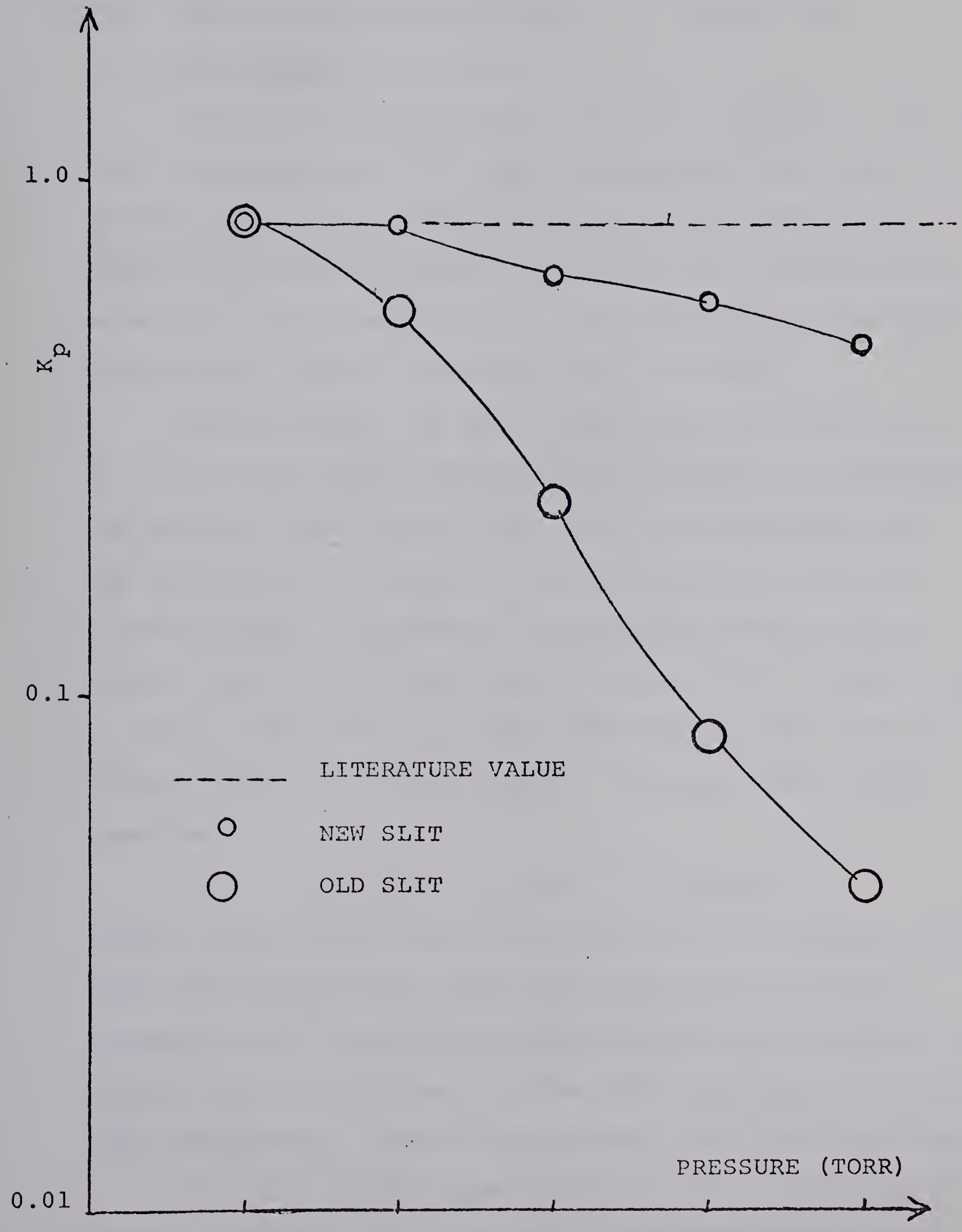

FIGURE (3:3)
The Equilibrium Constants of Water with the New and Old Ion Exit Slits

(B) Equilibrium Determinations with Narrowed Ion Exit Slit.

After it was shown that results in agreement with previous determinations for water could be obtained with the present apparatus, a series of experiments with ethanol vapour were made at several pressures and at various constant ion source temperatures. The equilibrium constants obtained are shown in Figures (3:4) to (3:10).

Unfortunately, as can be seen from the figures the K_p values still show a significant dependence on pressure. One source of the trouble that could be established was the ionization of ethanol by stray electrons outside of the ion source. Apparently the pressure outside the ion source was sufficiently high that some of the $C_2H_5OH^+$ formed by impact with stray electrons did collide with one more ethanol molecule giving $C_2H_5OH_2^+$. However, the further reaction,

$$C_2H_5OH_2^+ + C_2H_5OH \rightleftarrows (C_2H_5OH)_2H^+$$

cannot occur outside the ion source since it requires third body stabilization and cannot be operative at the low pressures (10^{-4} torr) prevailing outside the ion source. The reasons for the curvature in the other $K_{n-1,n}$ plots are not well understood. Some stripping must still be occurring.

In spite of the unsatisfactory nature of the equilibrium constants it was decided to construct Van't Hoff plots and obtain $\Delta H_{n-1,n}$ values.

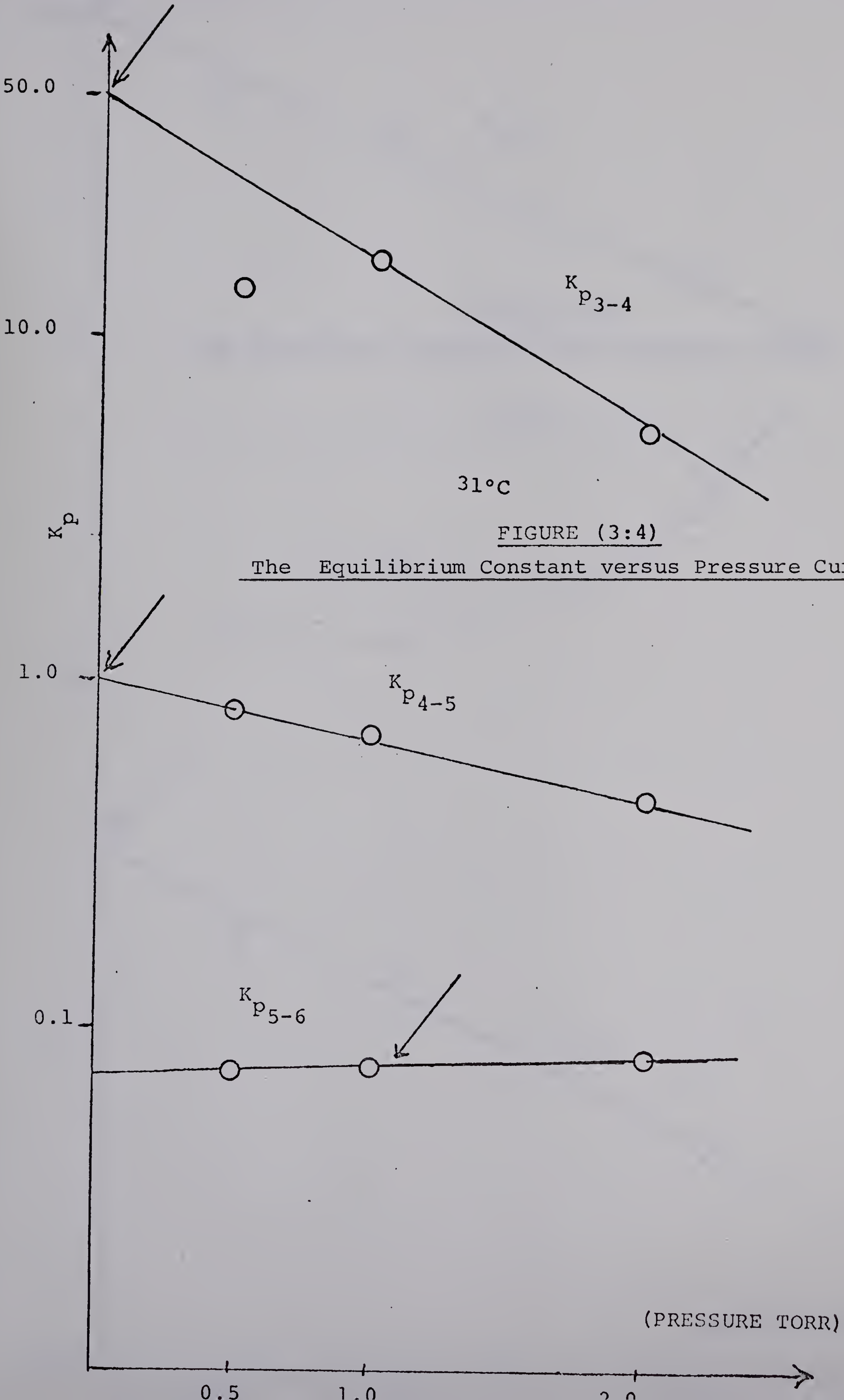

FIGURE (3:4)

The Equilibrium Constant versus Pressure Curves

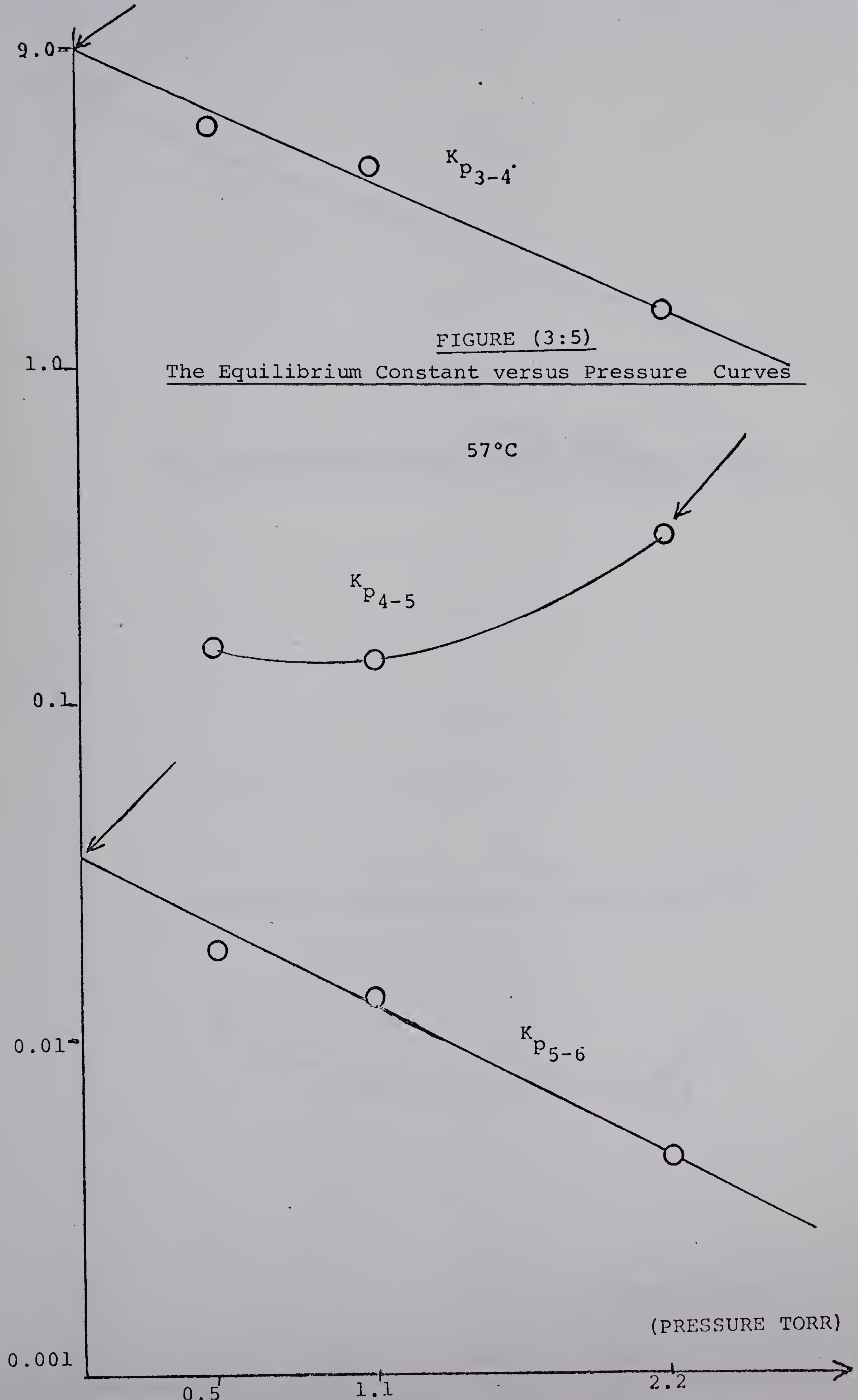

FIGURE (3:5)

The Equilibrium Constant versus Pressure Curves

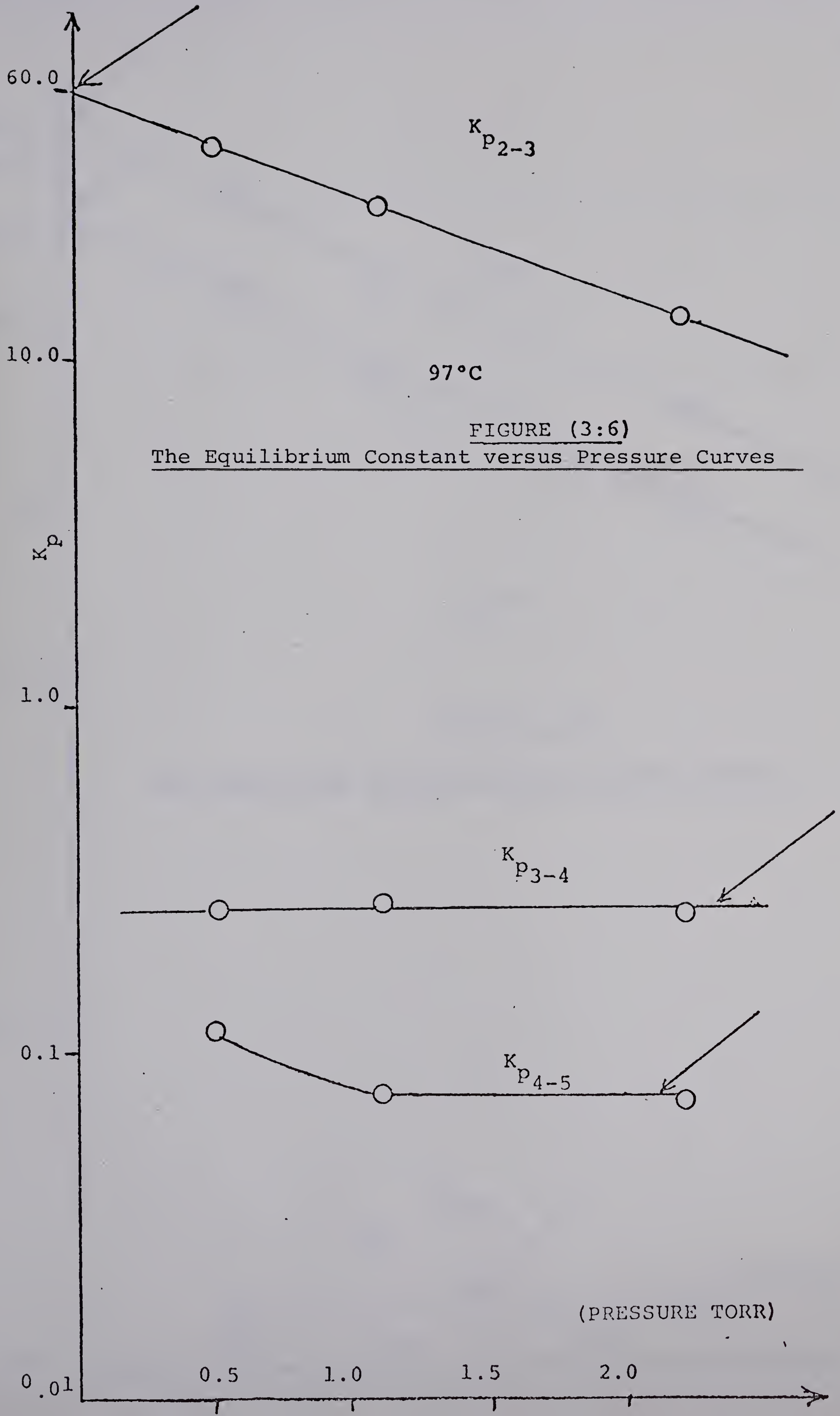

FIGURE (3:6)
The Equilibrium Constant versus Pressure Curves

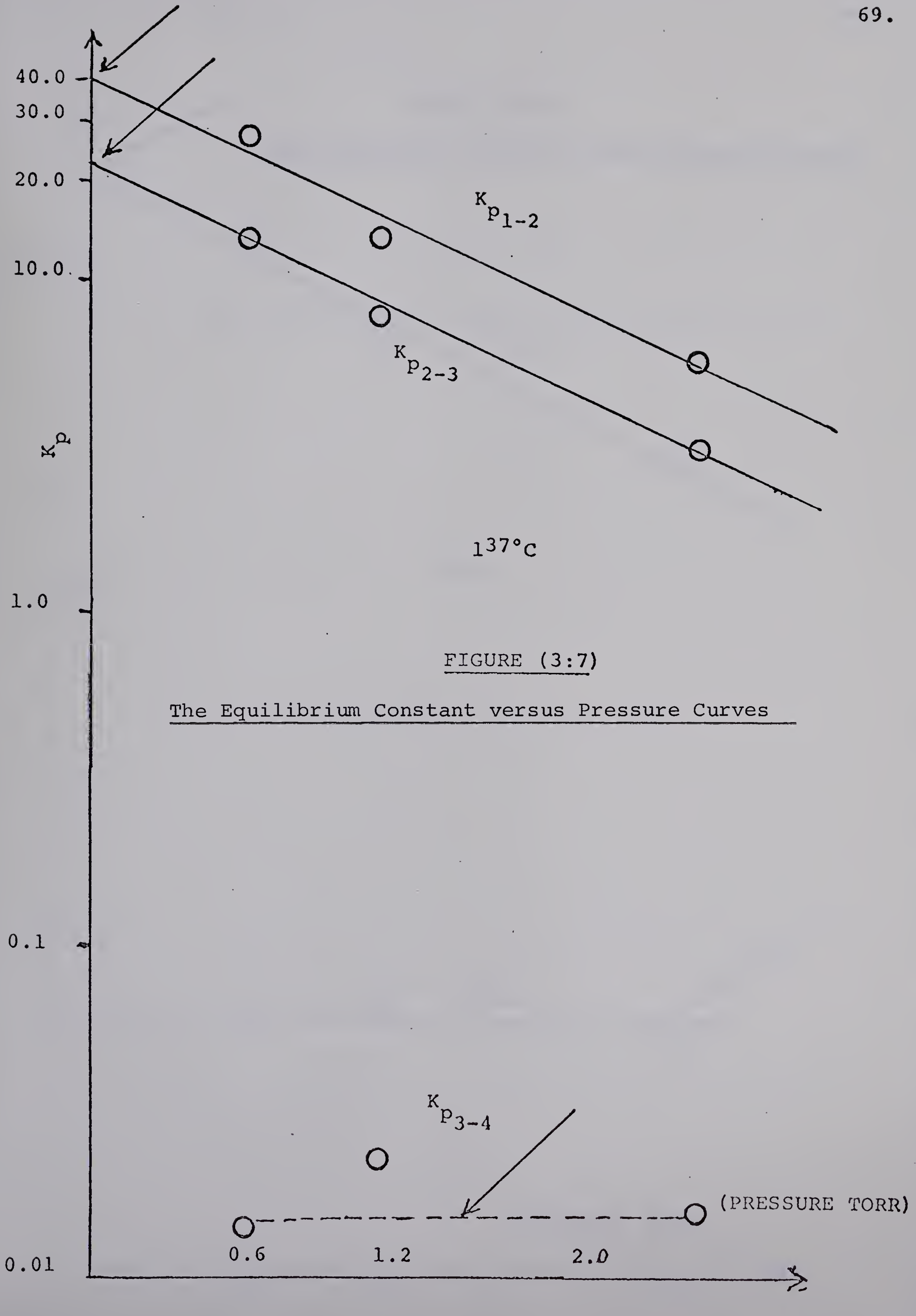

FIGURE (3:7)

The Equilibrium Constant versus Pressure Curves

FIGURE (3:8)

The Equilibrium Constant versus Pressure Curves

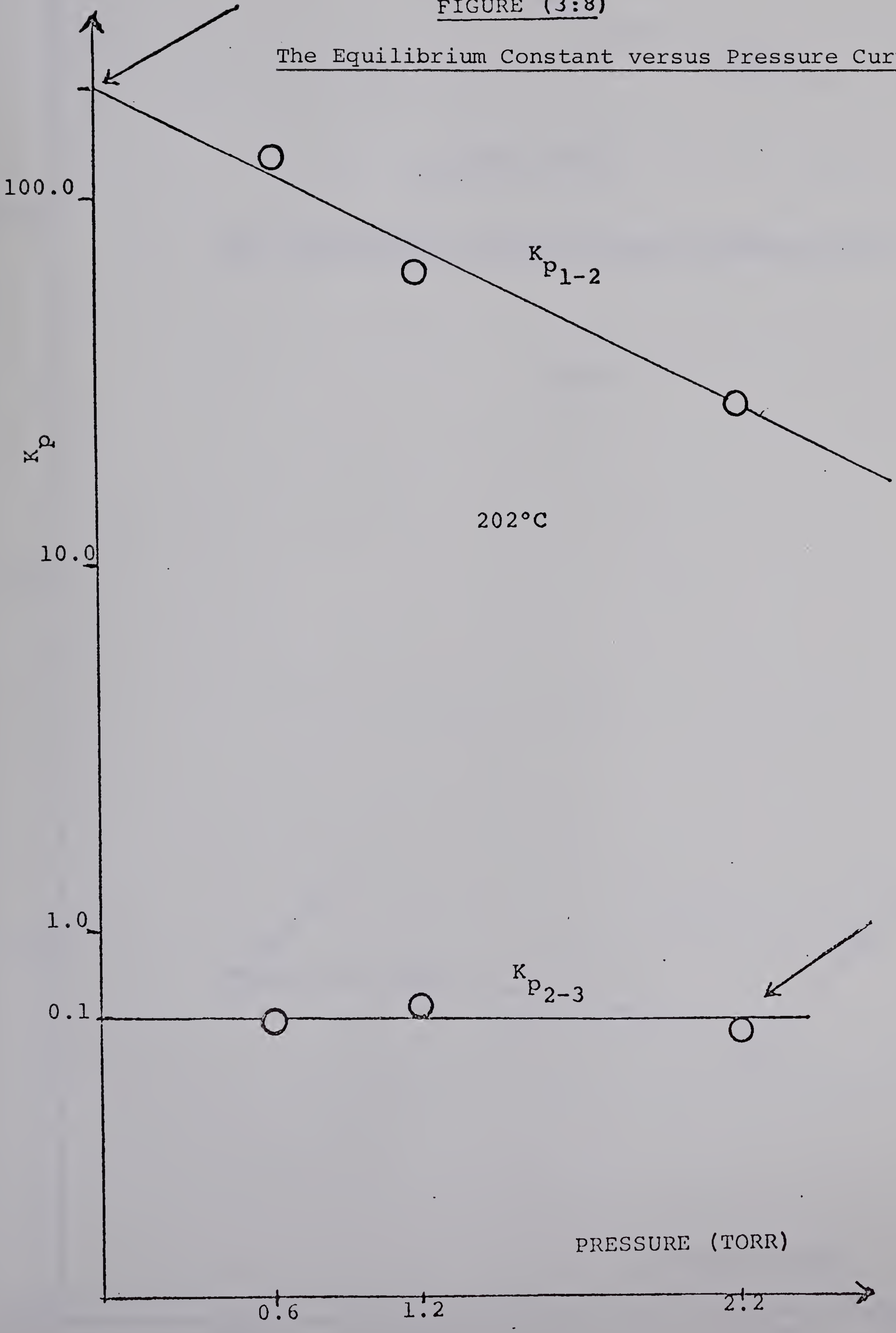

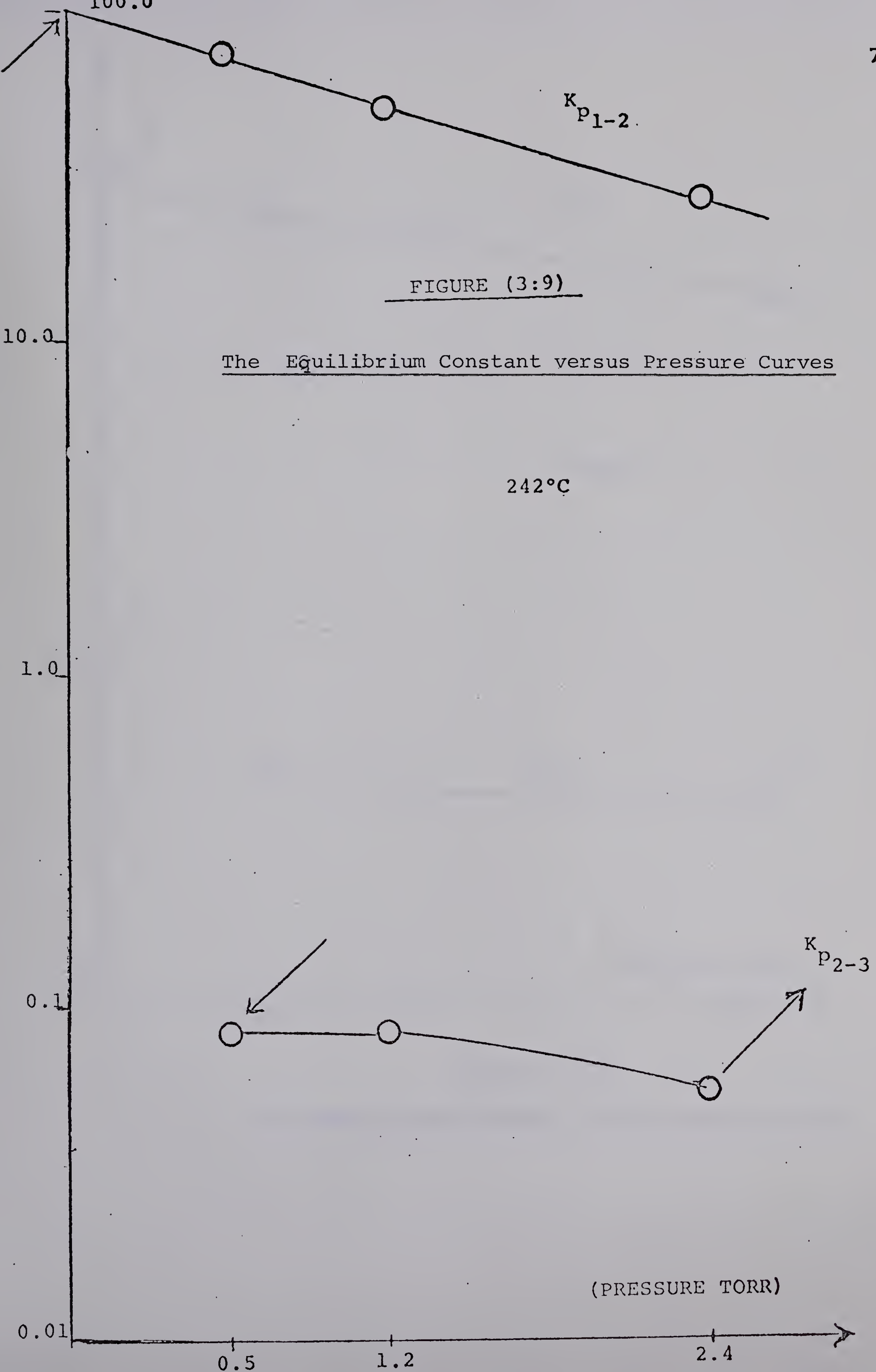

FIGURE (3:9)

The Equilibrium Constant versus Pressure Curves

242°C

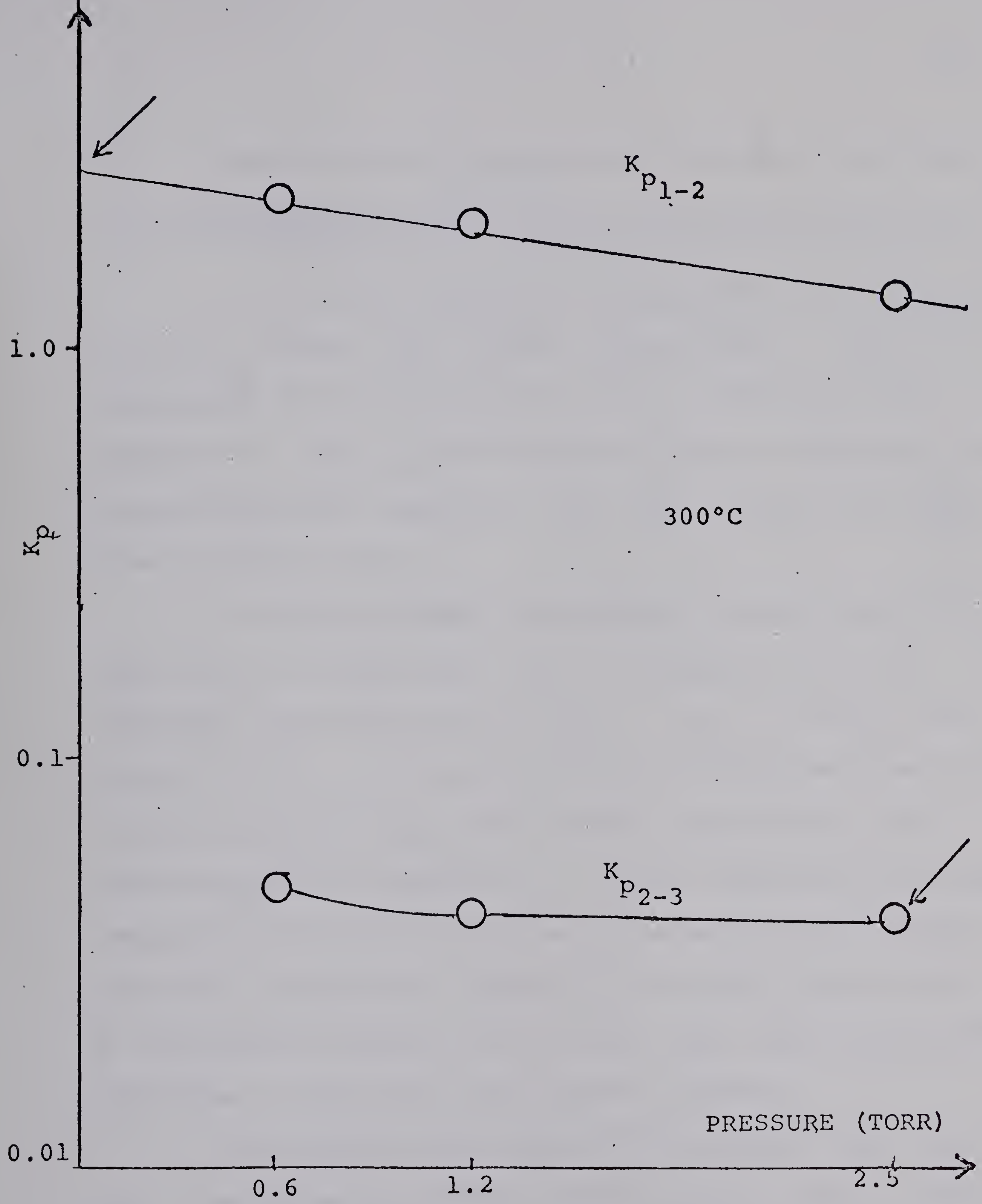

FIGURE (3:10)

The Equilibrium Constant versus Pressure Curves

3:3 Enthalpies and Entropies of Clustering Reactions in Ethanol.

The ΔH values could be obtained from the slopes of the log K_p versus (1/T) curves (Figure 3:12). The ΔG^o values were also evaluated from the K_p values for each temperature. The ΔS values were calculated utilizing the "Gibbs-Helmholtz" equation. All these values are tabulated in Table (3:2).

As can be noticed the enthalpy changes are of the right order of magnitude, and $-\Delta H$ decreases with the increasing size of cluster ($-\Delta H_{o,1} > \Delta H_{1,2} > -\Delta H_{2,3}$ etc..). Actually ($-\Delta H_{n-1,n}$) decreases with further growth because of the increasing importance of the dipole-dipole and molecule-molecule repulsions. A brief comparison regarding the heat of solvations between the water and the ethanol molecules as solvating agents of the proton can be made on the basis of Figure (3:12) which shows the corresponding enthalpies in the water and ethanol systems.

The higher ($-\Delta H$) values of ethanol for the (0,1), (1,2) reactions must be due to the greater proton affinity of ethanol compared to water. However, a gradual equalization is observed at (2,3), (3,4) stages. In the cases of higher clustering reactions (4,5), (5,6) the values of ethanol are appreciably lower than the values of water because of the crowding effect in ethanol is much bigger than in water.

TABLE 3:2

The ΔH, ΔG°_{298}, ΔS°_{298} values

n-1,n	$-\Delta H_{n-1,n}$ Kcal/mole	$-\Delta G^{\circ}_{298\,n-1,n}$ Kcal/mole	$-\Delta S^{\circ}_{298\,n-1,n}$ e.u.
0,1	193.0		
1,2	42	16.35	86.0
2,3	22.4	12.85	32.0
3,4	20.0	7.07	43.3
4,5	8.9	4.07	13.7
5,6	6.7	2.53	8.5

FIGURE (3:11)

Van't Hoff Plots

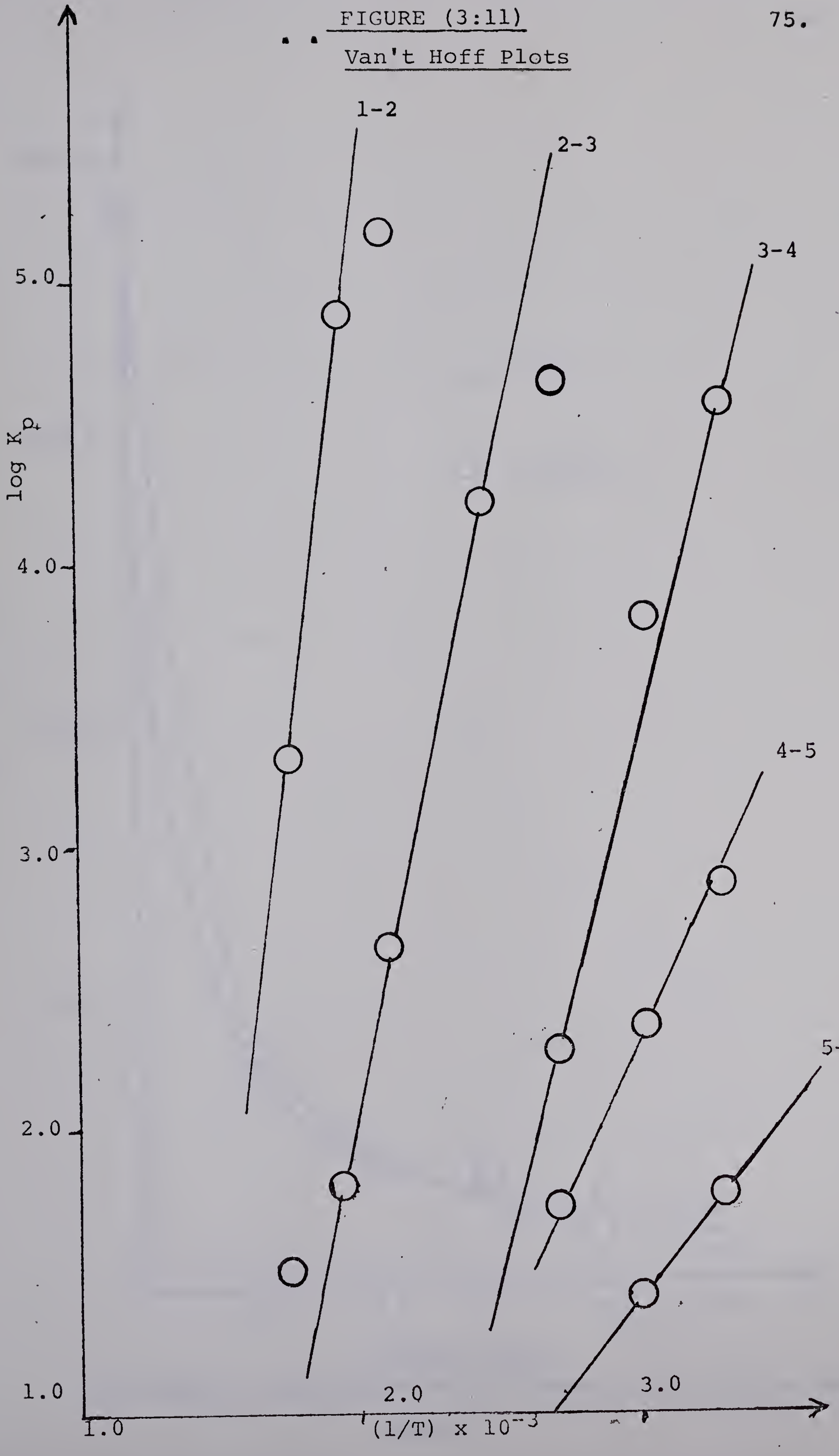

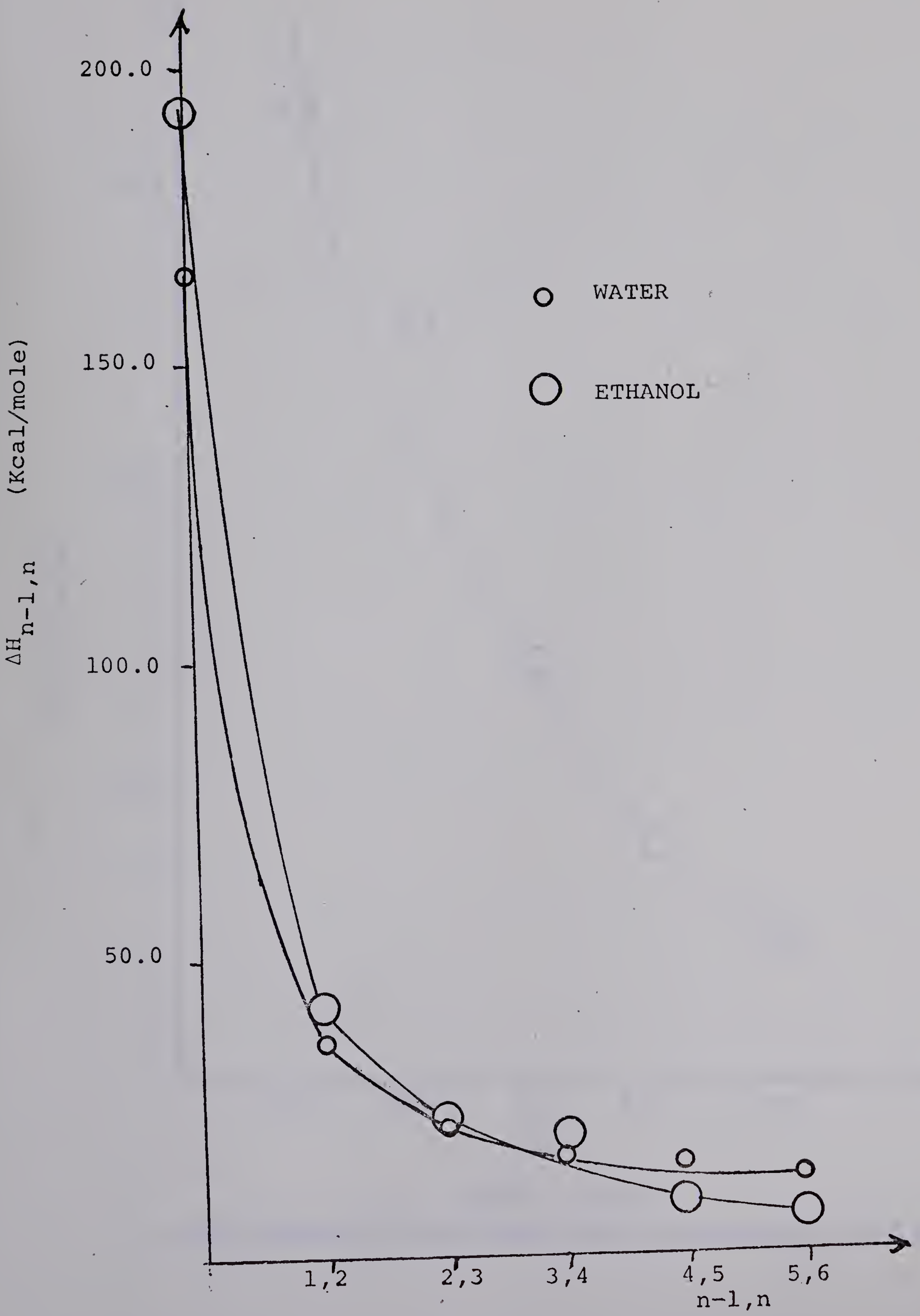

FIGURE (3:12)

The Change of Enthalpies with Cluster Size in Water and Ethanol

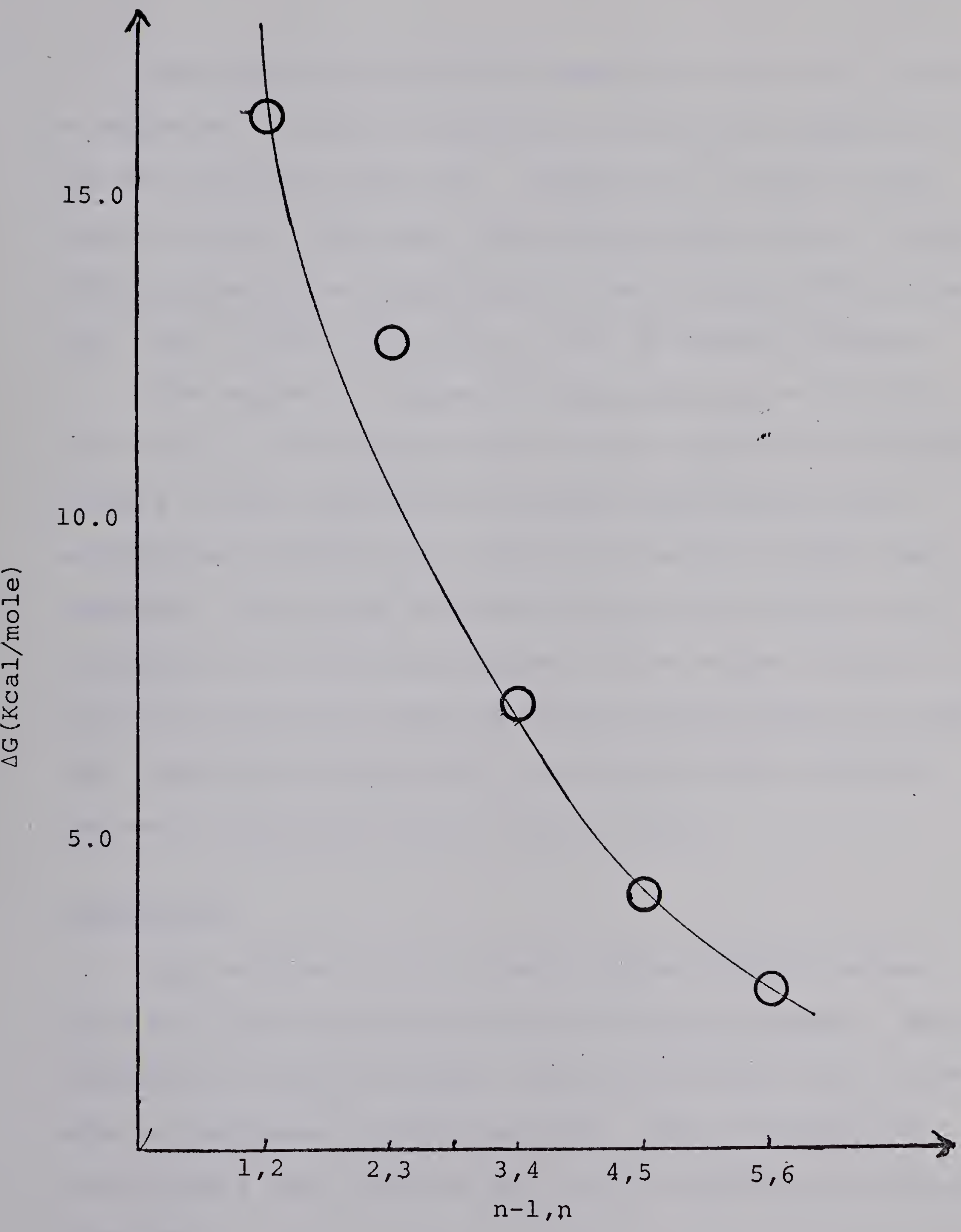

FIGURE (3:13)

The Change of Free Energy with Cluster Size in Ethanol

The ΔS values generally seem larger than what could be expected. The discrepancies are greatest especially for the first two reactions. Theoretical values of the granslational, rotational, and vibrational entropy changes for $\Delta S_{1,2}$ can be estimated and it can be shown that values for $-\Delta S_{1,2}$ larger than 40 e.u. are extremely unlikely.

The reason for these discrepancies may be the uncertainty in the determination of the equilibrium constants. Because of the significant pressure dependence of the equilibrium constants the right ones might not have been selected. This would of course cause some errors in the evaluation of ΔH and particularly of ΔG values (Figure 3:12). Since one has to use both of these derived values (ΔH) and (ΔG), which are large terms, to calculate the entropies, the resulting error could be quite large.

Conclusion

The derived ΔH are probably quite reliable since Van't Hoff plots generally tend to equalize errors. The ΔH values are in good agreement with predictions that can be made on the basis of previous work. The ΔG values are considerably less reliable and the ΔS results are probably incorrect.

Suggestions for Further Work

More accurate data related to the thermodynamic properties of the solvation reactions of the proton with ethanol and the kinetic properties of the system are planned

as the future goals of the project.

REFERENCES

1. J. J. Thomson, "Rays of Positive Electricity" P.32, Longmans, Green and Co., Ltd., London 1933.
2. A. J. Dempster, Phil. Mag., 31, 438 (1916)
3. M. M. Mann, A. Hustrulid, and J. T. Tate, Phy. Rev., 58, 340 (1940).
4. G. C. Eltenton, Monthly Reports of Shell Development Co., Emeryville, Calif., April 1940.
5. V. L. Tal'roze and A. K. Lyubimova, Doklady Akad. Nauk S.S.S.R., 86, 909 (1952).
6. D. P. Stevenson and D. O. Schissler, J. Chem. Phys., 23, 1353 (1955).
7. F. H. Field, J. L. Franklin and F. W. Lampe, J. Am. Chem. Soc., 79, 2419, 2665, 4244, 6129 (1957).
8. C. A. McDowell, "Mass Spectrometry", McGraw-Hill Book Company Inc., (1963).
9. P. J. Ausloos, "Ion-Molecule Reactions in the Gas Phase", Am. Chem. Soc., (1966).
10. R. W. Kiser, "Introduction to Mass Spectrometry" Prentice-Hall (1965).
11. A. G. Harrison and J. J. Myher, "Ion-Molecule Reactions in the Gas Phase" Am. Chem. Soc., (1966).
12. Gioumousis, G, Stevenson, D.P., J. Chem. Phys. 29, 294 (1958).
13. Stevenson, D.P., Schissler, D. O., J. Chem. Phys. 29, 287 (1958).

14. Field, F. H., Franklin, J. L., Lampe, F.W., J. Am. Chem. Soc., 79, 2419, 2665 (1957).

15. Field, F. H., Lampe, F. W., J. Am. Chem. Soc., 80 5583 (1958).

16. Moran, T. F., Hamill, W. H., J. Chem. Phys., 39, 1413 (1963).

17. Ryan, K. R., Futrell, J. H., J. Chem. Phys., 42, 824 (1965).

18. Berta, M.A., Koski, W.S., J. Am. Chem. Soc., 86, 5098, (1964).

19. Giese, C.F., Maier, W. B., J. Chem. Phys., 35, 1913 (1961).

20. Weiner, E.R., Hertel, G. R., Koski, W.S., J. Am. Chem. Soc., 86, 788 (1964).

21. Henglein, A., Muccini, G., Z. Naturforsch., 17a, 452 (1962).

22. Henglein, A., Muccini, G., Z. Naturforsch., 18a, 1753 (1963).

23. Markin, M.I., Tal'roze, V.L., Elementarnye Protsessy Khim. Vysokikh Energ. Akad. Nauk S.S.S.R. Inst. Khim. Fiz., Tr. Simposiuma, Moscow 1963, 18 (1965).

24. Tal'roze, V. L., Frankevich, E.L., Zhur. Fiz. Khim., 34, 2709 (1960).

25. A. Good, D. A. Durden and P. Kebarle, J. Chem. Phys., to be published, (1969).

26. Tal'roze, V.L., Pure Applied Chem., 5, 455 (1962).

27. Ryan, K. R., Sieck, L. W., and Futrell, J. H., J. Chem. Phys., 41, 111 (1964).

28. Sieck, L. W., Abramson, F. P., and Futrell, J. H., J. Chem. Phys., 45, 2859 (1966).

29. M. E. Russell and W. A. Chupka, J. Phys. Chem., to be published.

30. Koyano, I., Omura, I., and Tanaka, I., J. Chem. Phys., 44, 3850 (1965).

31. Bansal, K. M., Freeman, G. R., J. Am. Chem. Soc., 90, 7190 (1968).

32. Durden, D.A., Ph.D. Thesis, University of Alberta, Edmonton, (1969).

33. D. A. Durden, P. Kebarle, and A. Good, J. Chem. Physics, 50, 805, (1968).

34. Post, R. F., Henrich, A., UCRL Report 2209.

35. Paul, W., Steinwedel, H., Naturforsch 8a, 448, (1953).

36. P. Kebarle, S. K. Searles, A. Zolla, J. Scarborough, and M. Arshadi, J. Am. Chem. Soc., 89, 6393 (1967).

37. P. Kebarle, R. N. Haynes, and T. G. Collins, J. Am. Chem. Soc., 89, 5753 (1967).

38. P. Kebarle, Advances in Chemistry Series, Number 72, (1968).

39. S. K. Searles and P. Kebarle, Can. J. Chem., 47, 14 (1969).

APPENDIX

```
                       C    NORMALIZATION BY MATRIX METHOD (ISIL)

ISN 0002                    REAL H(27,9),TR(9),SF (9),CH(27,9),
                            TOT(27),P(27,9)

ISN 0003                    DATA TR /0.29,0.26,0.19,0.2,0.19,0.18,0.155,
                            0.11,0.08 /, ISF /5.75,5.50,4.95,4.55,
                            4.21,4.2,4.18,4.1,3.9 /
ISN 0004                    READ(5,3) H
ISN 0005                  3 FORMAT(16F5.0)
ISN 0006                    DO  7  M=1,9
ISN 0007                    DO  7  N=1,27
ISN 0008                  7 CH(N,M)=H(N,M)*(1/(TR(M)*SF(M)))
ISN 0009                    DO  15 N=1,27
ISN 0010                 15 TOT(N)=0.0
ISN 0011                    DO  17 N=1,27
ISN 0012                    DO  17 M=1,9
ISN 0013                 17 TOT(N)=TOT(N)+CH(N,M)
ISN 0014                    DO  37 N=1,27
ISN 0015                    DO  37 M=1,9
ISN 0016                 37 P(N,M)=CH(N,M)/TOT(N)
ISN 0017                    WRITE(6,5)  ((H(N,M),M=1,9),N=1,27)
ISN 0018                  5 FORMAT(9(5X,F5.0))
ISN 0019                    WRITE(6,13)  ((CH(N,M),M=1,9),N=1,27)
ISN 0020                 13 FORMAT(9(4X,F6.1))
ISN 0021                    WRITE(6,25) (TOT(N),N=1,27)
ISN 0022                 25 FORMAT((25X,F8.2))
ISN 0023                    WRITE(6,47) ((P(N,M),M=1,9),N=1,27)
ISN 0024                 47 FORMAT(9(5X,F5.3))
ISN 0025                     STOP
ISN 0026                    END

****** END OF COMPILATION *****
```

B29922